SEARCH FOR E_6 ISO-SINGLET QUARKS IN ATLAS, THROUGH THE $H\,J\,Z\,J$ DECAY CHANNEL

by

Ismet Sıral

B.S., Electronics Engineering, Sabanci University, 2012

Submitted to the Institute for Graduate Studies in
Science and Engineering in partial fulfillment of
the requirements for the degree of
Master of Science

Graduate Program in Physics

Boğaziçi University

2014

ACKNOWLEDGEMENTS

Foremost, I would like to give my deep gratitude to Erkcan Özcan and Gökhan Ünel for their immense efforts. They are the reason that I am on the track to become a high energy physicist. Also, I would like to thank my thesis committee: Ali Serkant Çetin and Metin Arık for their insight and patience.

Furthermore, I would like to thank , Merve Sahinsoy, Tulay Cuhadar Donszelmann, Serhat İstin and Mehmet Şahin. Without their help, support and ideas; this thesis wouldn't have existed.

Last but not least, I would like to thank my family for their patience, Sinan Kefeli for being beside me (even overseas) and the regular visitors of the Engin Arık lab for their friendship.

ABSTRACT

SEARCH FOR E_6 ISO-SINGLET QUARKS IN ATLAS, THROUGH THE $H\,J\,Z\,J$ DECAY CHANNEL

This thesis searches for the heavy iso-singlet quarks forseen by F. Gürsey, P. Ramond and P. Sikivie' s E_6 grand unified theory model using the data recorded by the ATLAS detector under the $pp \rightarrow DD \rightarrow HjZj \rightarrow 4j\,2l$ decay hypothesis. (a flavor changing neutral current process). The data used in the analysis corresponds to $20\,\mathrm{fb}^{-1}$ total integrated luminosity collected from proton proton collision at c.o.m. energy of 8 TeV, provided by the large hadron collider The analysis uses a cut based algorithm to select the events with four jets and a Z candidate that has been reconstructed from two charged leptons. Flavor tagging is used to improve the reconstruction of the Higgs bosons. No excess events beyond what is predicted by the Standard Model has been observed and the E_6 heavy iso-singlet quark with a mass lower then 490 GeV is excluded at 95% confidence level. Also no excess events beyond what is predicted by the Standard Model has been observed on the search for a heavy quark that decays only via flavor changing neutral currents. For this quark, the mass lower then 730 GeV is excluded with the 95% confidence level.

ÖZET

ATLAS DENEYİNDE E_6 ISO-SINGLET QUARKLARININ $H\,J\,Z\,J$ KANALINA BOZUNUMUN ARAŞTIRILMASI

Bu çalışmada F. Gürsey, P. Ramond ve P. Sikivie tarafından önerilmiş olan E_6 büyük birleşim kuramının öngördüğü ağır iso-singlet kuarklar, $pp \rightarrow DD \rightarrow HjZj \rightarrow 4j\,2l$ kanalında aranmıştır. Bu araştırmada CERN'deki Büyük Hadron Çarpıştırıcısı'nda 8 TeV kütle merkezi enerjisinde üretilen proton proton çarpışmaları kullanılmıştır. Tamamı $20\,\mathrm{fb}^{-1}$ entegre ışınlığa denk gelen ve ATLAS dedektörü ile kaydedilmiş çarpışma verisi içinde yüklü lepton çiftlerinden Z bozonu, en az biri çeşni işaretlenmesi yapılmış olan iki jetten de Higgs bozonu yapılandırılmıştır. Standart Model'in beklentilerinden herhangi bir sapma gözlenmemiştir ve E_6 ağır iso-singlet kuark kütlesi 490 GeV'e kadar 95% güvenilirlik düzeyinde dışarlanmıştır. Sadece çeşni değiştiren nötr akımlara bozunan ağır kuarklar ise 730 GeV'e kadar 95% güvenilirlik düzeyinde dışarlanmıştır.

TABLE OF CONTENTS

LIST OF FIGURES

LIST OF TABLES

LIST OF SYMBOLS

A_μ	Electromagnetic Field
b , $\bar{b}$	Bottom Quark
c , $\bar{c}$	Charm Quark
D_μ	Gauge Covariant Derivative
d_0	Transverse distance between track and the beam axis
D_H	The Reconstructed D Quark From a H Quark
D_Z	The Reconstructed D Quark From a Z Quark
d , $\bar{d}$	Down Quark
D , $\bar{D}$	Down Type Iso-Singlet Quark
E_T^{miss}	Missing Transverse Energy
E_T	Transverse Energy
e , $\bar{e}$	Electron (Lepton)
$F_{\mu\nu}$	Electromagnetic Field Tensor
H	Higgs Boson
j	Jet
l	Lepton
L	Luminosity
$\mathcal{L}$	Lagrangian
m_{Higgs}^{real}	Nominal Mass Of The Higgs Boson
$m_{D_H}^{reco}$	Mass Of The Reconstructed D_H Quark Candidate
$m_{D_Z}^{reco}$	Mass Of The Reconstructed D_Z Quark Candidate
m_{Higgs}^{reco}	Mass Of The Reconstructed Higgs Boson Candidate
m	Mass
P_T	Transverse Momentum
p	Proton
q	Quark / Quark Field
R	Radius Of a Particle Cone
s , $\bar{s}$	Strange Quark

t , $\bar{t}$	Top Quark
u , $\bar{u}$	Up Quark
W^{μ}	Massless Gauge Fields Which Form The Weak Vector Bosons
$W^{\pm}$	W Boson
z_0	Longitudinal distance between track and the beam axis
Z	Z Boson
$\chi^2_{E_6}$	Calculated χ^2 Value For The E_6 Quarks
χ^2_{Higgs}	Calculated χ^2 Value For the Higgs Boson
η	Polar Angle
γ^{μ}	Dirac Matrices
μ , $\bar{\mu}$	Muon (Lepton)
ν_{μ} , $\bar{\nu_{\mu}}$	Muon Neutrino
ν_{τ} , $\bar{\nu_{\tau}}$	Tau Neutrino
ν_{e} , $\bar{\nu_{e}}$	Electron Neutrino
ϕ	Azimuthal Angle
ψ	Fermion Field
σ_{D_H}	Reconstructed Width Of The D_H Quark
σ_{D_Z}	Reconstructed Width Of The D_Z Quark
σ_H	Reconstructed Width Of The Higgs
τ , $\bar{\tau}$	Tau (Lepton)
θ	Pseudo-rapidity
φ	Mixing Between the d and D quarks

LIST OF ACRONYMS/ABBREVIATIONS

ALICE	A Large Ion Collider Experiment
ATLAS	A Toroidal LHC Apparatus
CMS	The Compact Muon Solenoid
CMS	The Compact Muon Solenoid
CP	Charge Parity
CSC	Cathode Strip Chamber
EM	Electromagnetic
FCal	Forward Calorimeter
GRL	Good Run List
GUT	Grand Unified Theory
ID	Inner Detector
JES	Jet Energy Scaling
JVF	Jet Vertex Fraction
LAr	Liquid Argon
LB	Luminosity Block
LCW	Local Cluster Weighting
LHC	Large Hadron Collider
LHCb	Large Hadron Collider beauty
LHCf	Large Hadron Collider Forward
LINAC	Linear Particle Accelerator
MC	Monte Carlo
MDT	Monitored Drift Tube
MoDEAL	Monopole and Exotics Detector at the LHC
MS	Muon System
$\overline{\text{MS}}$	modified minimal subtraction
NLO	Next-To-Leading Order
NNLO	Next-to-Next-To-Leading Order
PS	Proton Synchrotron

PSB	Proton Synchrotron Booster
PV	Primary Vertices
QCD	Quantum Chromodynamics
QED	Quantum Electrodynamics
QFT	Quantum Field Theory
ROB	Read Only Buffers
RPC	Resistive Plate Chamber
SCT	Semi-Conductor Tracker
SM	Standard Model
SPS	Super Proton Synchrotron
TDAQ	Trigger And Data Acquisition
TGC	Thin Gap Chamber
TOTEM	TOTal Elastic and diffractive cross section Measurement
TRT	Transition Radiation Tracker

1. INTRODUCTION

The LHC is currently the worlds most powerful particle collider with a 8 TeV center of mass energy, and it is the recent discoverer of the Higgs boson (observed in ATLAS and CMS experiments). With this discovery , new opportunities for new physics has emerged and this thesis aims to search for heavy iso-singlet quarks proposed in the E_6 GUT theory using the newly discovered Higgs boson in the ATLAS detector.

The SM model theory is a near complete theory, but within it's framework it cannot unify the fundamental forces. For this reason grand unified theories (GUT) tries to unify all the fundamental forces except gravity (some GUT theories also includes unification of the gravity like E_7). One of these GUT theories is the F. Gürsey, P. Ramond and P. Sikivie' s E_6 model. The theory predicts a heavy iso-singlet quark for each quark family. These heavy iso-singlet quarks are expected to be highly unstable decaying in to quarks in it's family via the mechanisms $D \to V, j$ where $V = (H, Z, W^{\pm})$.

In this thesis the iso-singlet quark pair generation and it's immediate decay via the $pp \to DD \to HjZj \to 4j\,2l$ mechanism is examined. This thesis uses the data from ATLAS detector with the specifications of $20\,\mathrm{fb}^{-1}$ proton proton collusions at $\sqrt{s} = 8\,\mathrm{TeV}$ recorded till the end of 2012 in LHC. In this thesis, the event selection is done using a cut based technique and the event reconstruction is done using a χ^2 algorithm and with the reconstruction of a Z candidate using two leptons.

The backgrounds are generated according to the SM using Monte Carlo simulations and the background rejection is done using the tool MCLimit that uses the CL_S method.

2. THEORY

2.1. Elementary Particles

Within our current knowledge, the smallest building blocks of our universe are the elementary particles (fundamental particles). They are classified according to their spin. The half integer spin particles are called fermions and they obey the Fermi-Dirac statistics. The integer spin particles are called bosons and they obey the Bose-Einstein statistics.

Fermions are the building blocks of our observed matter since they obey the Fermi-Dirac statistics. They are categorized into two distinct types: quarks and leptons. Quarks carry color and Coulomb charges and they can interact via all known forces. Leptons on the other hand carry only Coulomb charges thus they cannot interact through the strong force. The fermions are also divided into 3 generations of particle families each of which is composed of two different doublets. Finally each fermion has its anti-pair. The list of all particles and their properties can be found in Table 2.1. The leptons in nature can exist alone but quarks cannot. Instead quarks combine with each other forming composite particles called baryons and mesons. Baryons are composed of three different quarks with different color charges forming a colorless particle (example: proton) and mesons are composed of a quark-antiquark pair with opposite color charges forming a colorless particle (example: $\pi^{0,\pm}$).

Bosons are the carriers of the fundamental forces in our universe. Currently there are five observed bosons, and they are associated with three of the fundamental forces: electromagnetic, weak and strong forces. There is also a proposed boson associated with the gravitational force but it hasn't been observed yet. The electromagnetic(EM) force is the force that binds the electrons' orbits around the atoms and is mediated with the photon. The strong force is responsible for the color charge interaction, it is the force that binds hadrons together and it is mediated by the gluon (g). Lastly there is

Table 2.1. List Of All Known Fermions, According To PDG [3].

Name	**Particle**	**Anti-Particle**	**Type**	**Family**	**Charge (e)**	**Mass (MeV)**
up	u	$\bar{u}$	quark	1^{st} gen.	+2/3	$2.3^{+0.7}_{-0.5}$
down	d	$\bar{d}$	quark	1^{st} gen.	-1/3	$4.8^{+0.5}_{-0.3}$
charm	c	$\bar{c}$	quark	2^{nd} gen.	+2/3	1275 ± 25
strange	s	$\bar{s}$	quark	2^{nd} gen.	-1/3	95 ± 5
top	t	$\bar{t}$	quark	3^{rd} gen.	+2/3	173070 ± 720
bottom	b	$\bar{b}$	quark	3^{rd} gen.	-1/3	$4180 \pm 30\,(\overline{\text{MS}})$
electron	e^-	e^+	lepton	1^{st} gen.	-1	0.511
electron neutrino	ν_e	$\bar{\nu_e}$	lepton	1^{st} gen.	0	< 0.0000022
muon	μ^-	μ^+	lepton	2^{nd} gen.	-1	105.7
muon neutrino	ν_μ	$\bar{\nu_\mu}$	lepton	2^{nd} gen.	0	< 0.170
tau	τ^-	τ^+	lepton	3^{rd} gen.	-1	1777
tau neutrino	ν_τ	$\bar{\nu_\tau}$	lepton	3^{rd} gen.	0	< 15.5

Table 2.2. List Of All Known Bosons. According To PDG [3].

Name	Particle	Force	Charge (e)	Mass (GeV)	Width (GeV)
photon	γ	electromagnetic	0	0	0
gluon	g	strong	0	0	0
Higgs	H	N/A	0	125.9 ± 0.4	< 0.01 [4]
Z boson	Z	weak	0	91.188 ± 0.002	2.495 ± 0.002
W boson	$W^\pm$	weak	± 1	80.39 ± 0.015	2.085 ± 0.042

the weak force which is mediated by the Z, $W^\pm$ bosons. The weak force is responsible for the decays of various particles, such as the radioactive decays of the nuclei. There exists one more boson which is not associated with any of the fundamental forces, the newly discovered Higgs boson. The Higgs boson is responsible for the masses of the fundamental particles, and for breaking the electroweak symmetry. The list of all bosons can be found in Table 2.1.

2.2. The Standard Model

The Standard Model (SM) is currently the most successful theory in particle physics, being able to predict experimental results with high accuracy. It is quantum field theory (QFT) that successfully incorporates all observed fermions and bosons. The group structure of the SM is $SU_C(3) \times SU_W(2) \times U_Y(1)$ where the

$SU_C(3)$ corresponds to the strong interaction and the $SU_W(2) \times U_Y(1)$ stands for the weak+electromagnetic interactions. The SM doesn't incorporate the gravity, and this issue is a hot research topic in theoretical physics. The Standard Model can itself be studied under into four titles depending on the interactions of various bosons / fields.

2.2.1. Quantum Electrodynamics

The electromagnetic interactions of the SM are explained by the quantum electro dynamics (QED). The QED Lagrangian can be found at Equation 2.1.

$$\mathcal{L}_{QED} = \bar{\psi}[i\gamma^{\mu}(\partial_{\mu} - ieA_{\mu}) - m]\psi - \frac{1}{4}F^{\mu\nu}F_{\mu\nu} \tag{2.1}$$

This Lagrangian shows the interaction of a fermion field ψ of charge e with the electromagnetic field A_{μ}. QED theory can predict experimental results with extremely high precision.

2.2.2. Weak Interactions

With the discovery of the β decay Enrico Fermi proposed the weak interaction which allowed the electrons to interact with neutrinos. This interaction can be modeled by combining a charged lepton field (ex. electron) with it's corresponding neutrino field under a doublet form. This doublet form allows the mixing of these two fields and transformations can be defined to account for the mixing.

$$\psi \rightarrow \begin{pmatrix} \psi_1 \\ \psi_2 \end{pmatrix} \text{ and } \psi' = e^{\vec{\theta}\cdot\vec{\tau}}\psi \tag{2.2}$$

This new doublet should be locally invariant. The Lagrangian that satisfies these properties can be found on Equation 2.3.

$$\mathcal{L}_{YM} = \bar{\psi}[i\gamma^{\mu}D_{\mu} - m]\psi - \frac{1}{4}F_i^{\mu\nu}F_{\mu\nu}^i \tag{2.3}$$

In this equation the $D_\mu = \partial_\mu - ig\vec{W}_\mu \cdot \vec{\tau}$ where W_μ stands for massless gauge fields which form the weak vector bosons and $F^i_{\mu\nu} = \partial_\mu W^i_\nu - \partial_\nu W^i_\mu + g\epsilon_{ijk} W^j_\mu W^k_\nu$.

This theory assumes that the weak vector bosons are massless which is experimentally disproved.

2.2.3. Electroweak unification

The experimental observations showed that the charged weak interactions coupled only to the left handed fermions. To account for this observation the field spinor was combined with the axial vector forming the chiral fermion states that can be found on Equation 2.4. According to the chiral spinors, now the charged fermions could only couple to left handed particles.

$$\psi_L = \frac{1-\gamma^5}{2}\psi \; ; \; \psi_R = \frac{1+\gamma^5}{2}\psi \tag{2.4}$$

Using these chiral fermions and forming a left handed neutrino, charged lepton doublet the $SU(2)_L$ group can be formed. When electromagnetic interactions are added to the equation the group $SU(2) \times U(1)$ is formed. The Lagrangian for the electroweak theory can be found on Equation 2.5. The Equations 2.6, 2.7, 2.8 shows the fields for the bosons associated with electroweak interactions.

$$\mathcal{L}_{EW} = \bar{\psi} i\gamma^\mu D_\mu \psi - \frac{1}{4} W^i_{\mu\nu} W^{\mu\nu}_i - \frac{1}{4} B_{\mu\nu} B^{\mu\nu} \tag{2.5}$$

$$A_\mu = W^3_\mu \sin\theta_W + B_\mu \cos\theta_W \tag{2.6}$$

$$Z_\mu = W^3_\mu \cos\theta_W - B_\mu \sin\theta_W \tag{2.7}$$

$$W_{\mu}^{\pm} = \frac{1}{\sqrt{2}}(W_{\mu}^{1} \mp W_{\mu}^{2}) \tag{2.8}$$

2.2.4. Quantum Chromodynamics

Quantum Chromodynamics(QCD) corresponds to the $SU_C(3)$ group of the SM. It models the interaction of the color charged particles with gluons with the Lagrangian in Equation 2.9.

$$\mathcal{L}_{QCD} = \bar{q}[i\gamma^{\mu}D_{\mu} - m]q - \frac{1}{4}G_{\mu\nu}^{a}G_{a}^{\mu\nu} \tag{2.9}$$

The gauge fields observed with this theory should be massless which is in agreement with what is observed in nature. In addition to being massless the QCD also has two important properties.

The first property is the color confinement which states that the color charged particles cannot be isolated. The second property is the asymptotic freedom which states that at high energies the quarks interact with gluons weakly.

2.2.5. Higgs Mechanisms

In theory the newly obtained gauge bosons do not have mass, but experimentally the Z and $W^{\pm}$ are observed to have masses. In order to explain this the Higgs mechanism was proposed. To explain the working mechanism of the Higgs boson a sample scalar field's Lagrangian would be used.

A massless scalar field's Lagrangian with a potential energy term can be found at Equation 2.10. If the μ^2 term in this Lagrangian is negative, the minima of this Lagrangian lies at $\phi = \pm\sqrt{\frac{-\mu^2}{\lambda}}$. If this equation is expanded around the minima points, the Lagrangian transforms to the Equation 2.11. Here the $2\mu^2$ term acts as a mass term for the massless scalar field, which shows how particles can gain mass

through symmetry breaking. Although in this newly obtained Lagrangian expanded around the minima breaks the symmetry of the field.

$$\mathcal{L} = \partial_\mu \phi \partial^\mu \phi - \mu^2 \phi^2 + \lambda \phi^4 \tag{2.10}$$

$$\mathcal{L} = \partial_\mu \phi \partial^\mu \phi + 2\mu^2 \phi^2 + O(\phi^3) \tag{2.11}$$

Vector bosons also gains mass through the same mechanism. A similar Lagrangian can be derived for vector fields and which such Lagrangian, the observed masses of the Z and $W^\pm$ can be explained.

2.3. The Grand Unified Theory

With the discovery of Higgs, the Standard Model can be said to be complete but the current Standard Model has some undesirable features and lack an explanation to where its many parameters come from. The grand unified theories (GUTs) builds up on the existing SM theory. The first GUT was proposed by Howard Georgi and Sheldon Glashow in 1974 [5], with a model that unified all the fundamental forces except gravity. The group structure of the SM, $SU_C(3) \times SU_W(2) \times U_Y(1)$ holds the fundamental forces separate. The first GUT theory proposed that; the $SU(5)$ model could unify all the forces in the SM while the $SU(5) \supset SU_C(3) \times SU_W(2) \times U_Y(1)$. This theory proposed new interactions between the quarks and leptons via the two newly proposed bosons X and Y that holds the charges $+\frac{4}{3}$ and $+\frac{1}{3}$. The newly proposed particles by the $SU(5)$ also allows the proton to decay, which haven't been observed yet. This puts a mass constraint of $M_{X,Y} \approx 10^{16}\,\text{GeV}$ on the bosons. With this mass expectation, currently the technology is far from being able to prove this theory but there are other GUT theories that could unify all the fundamental forces. One of such theories is the F. Gürsey, P. Ramond and P. Sikivie's E_6 model [6].

2.4. The E_6 Model

Feza Gürsey's E_6 GUT theory proposes to use the mathematical E_6 model as the group structure. E_6 is the only only exceptional Lie group that has complex representations, hence it can entertain chiral fermions. The theory uses E_6's $SU_L(3) \times SU_R(3) \times SU_C(3)$ as a maximal compact subgroup unifying all the quarks and leptons into a forming a 27 multiplet [6]. This theory predicts a new quark and a charged lepton for each family. The newly proposed quark is an iso-singlet with the charge $-\frac{1}{3}$ and the newly proposed lepton has the charge of -1. The newly proposed quark adds an additional weak interaction term to the SM's Lagrangian. The addition Lagrangian term can be found in Equation 2.12. In this Lagrangian, D denotes the iso-singlet quark, φ stands for the mixing between the d and D quarks and θ stands for the CKM quark mixing. [7]

$$\mathcal{L}_D = \frac{\sqrt{4\pi\alpha_{em}}}{2\sqrt{2}\sin\theta_W}[\bar{u}^\theta\gamma_\alpha(1-\gamma_5)d\cos\varphi + \bar{u}^\theta\gamma_\alpha(1-\gamma_5)D\sin\varphi]W^\alpha - \frac{\sqrt{4\pi\alpha_{em}}}{4\sin\theta_W}[\frac{\sin\varphi\cos\varphi}{\cos\theta_W}\bar{d}\gamma_\alpha(1-\gamma_5)D]Z^\alpha + h.c \quad (2.12)$$

Since the newly proposed quark is iso-singlet, it doesn't directly interact with the Higgs boson and its mass is a result of a different mechanic but the iso-singlet quark still interacts with the Higgs field because of its mixing with the d quark. The iso-singlet quarks Higgs Field interaction is modeled by the following Lagrangian at Equation 2.13. In the equation h stands for the expansion of the Higgs around the new minimum of υ with the equation $H = \upsilon + h$ [8].

$$\mathcal{L}_h^M = \frac{m_D}{\upsilon}\sin^2\varphi_L\bar{D}^M D^M h - \frac{\sin\varphi_L\cos\varphi_L}{2\upsilon}\bar{D}^M[(1-\gamma^5)m_D + (1+\gamma^5)m_d]d^M h - \frac{\sin\varphi_L\cos\varphi_L}{2\upsilon}\bar{d}^M[(1+\gamma^5)m_D + (1-\gamma^5)m_d]D^M h + \frac{m_d}{\upsilon}\cos^2\varphi_L\bar{d}^M d^M h \quad (2.13)$$

According to the modified Lagrangian, the iso-singlet quark interacts with the

Z , $W^{\pm}$ and H bosons. For an iso-singlet quark at 300 GeV and for the Higgs Mass at 125 Gev the branching ratio for the W boson is 52% , Z boson is 29% and the Higgs boson is 19%. These values are calculated with CompHep by Serhat Istin on his soon to be published thesis [1]. The figure 2.1 plots the branching ratios of the iso-siglet quark for different masses.

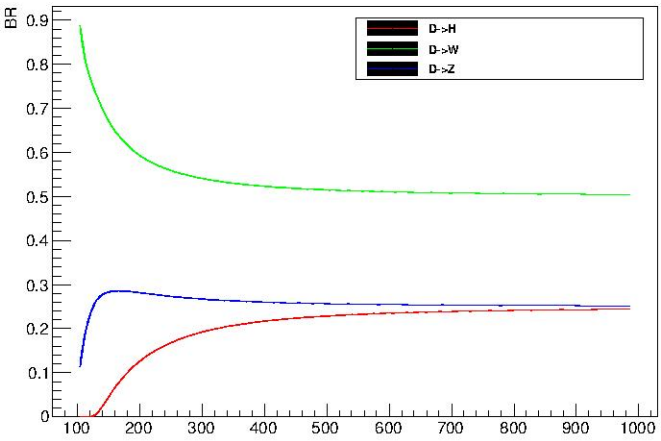

Figure 2.1. Branching Ratios VS Mass Of The Iso-Singlet Quark [1].

E_6 model is still a hot topic in physics. The possibilities of the model are still being examined. In 2011 a paper by Borut Bajc, Vasja Susič [9] is published searching for more realistic super-symmetric E_6 group model that can directly break in to the SM's gauge group.

2.5. The Search For The Iso-Singlet Quark

2.5.1. Production At ATLAS

The iso-singlet quark is expected to be pair produced in ATLAS via the following Feynman diagrams show in figure 2.5.1. The total cross section of these histograms at 8 TeV center of mass energy in the ATLAS detector can be found in figure 2.3. These cross-section values have been calculated with the HATHOR tool [10] and are the generic cross-sections for a pair produced heavy quark.

The pair produced iso-singlet guarks are not stable, thus they decay in to SM quarks via the allowed mechanisms by the E_6 Lagrangian. This results in 6 different decay channels for the iso-singlet quark pair: 2 jets and 2 bosons (HH, HZ, HW, ZZ, WZ, WW). In this thesis the leptonic decay of the HZjj channel is examined.

2.5.2. The Leptonic HZ Channel Of The Iso-Singlet Quark

The signal analyzed in this analysis is the pair produced iso-singlet quark decaying into a H-Z channel where the Z boson decays in the leptonic channel. The Feynman diagram for the decay of the pair produced iso-singlet quark can be found in the figure 2.4. In this channel 4 jets and a lepton pair is expected as a Signal. The two of the expected jets must have a high momenta while they are the direct decay products of the iso-singlet quarks. The other two jets are expected to be b-tagged while the standard model higgs has $\approx 60\%$ decay rate to a $b\bar{b}$ pair.

Among all the decay channels, the iso-singlet quark pair at a mass of 300 GeV has a 11% probability of decaying into a H,Z boson. The Z boson has a chance of 3.36% to decay in to an electron pair and 3.36% to a muon pair. So the probability of a iso-singlet quark pair decaying into a leptonic HZ channel is 0.7%. At $20\,\mathrm{pb}^{-}1$ for a 300 GeV iso-singlet quark, it is expected to see ≈ 1800 signal events at the ATLAS detector.

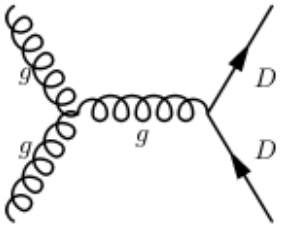

gluons, s channel

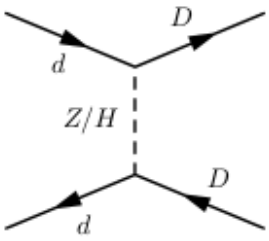

down quark, t channel 1

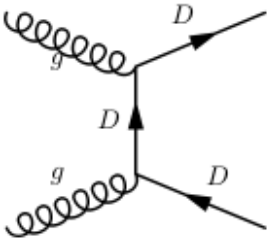

gluons, t channel

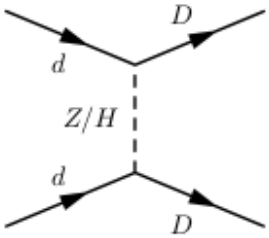

down quark, t channel 2

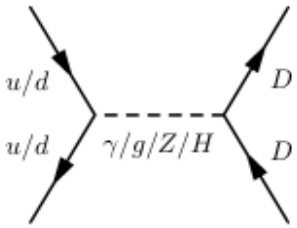

up / down quark, s channel

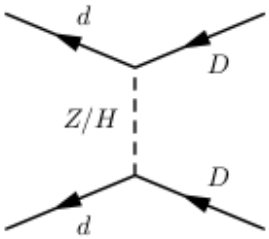

down quark, t channel 3

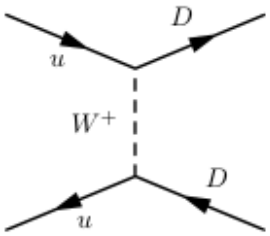

up quarks, t channel

Figure 2.2. The Feynman Diagrams Associated With Pair Production Of E_6 Iso-Singlet Quarks.

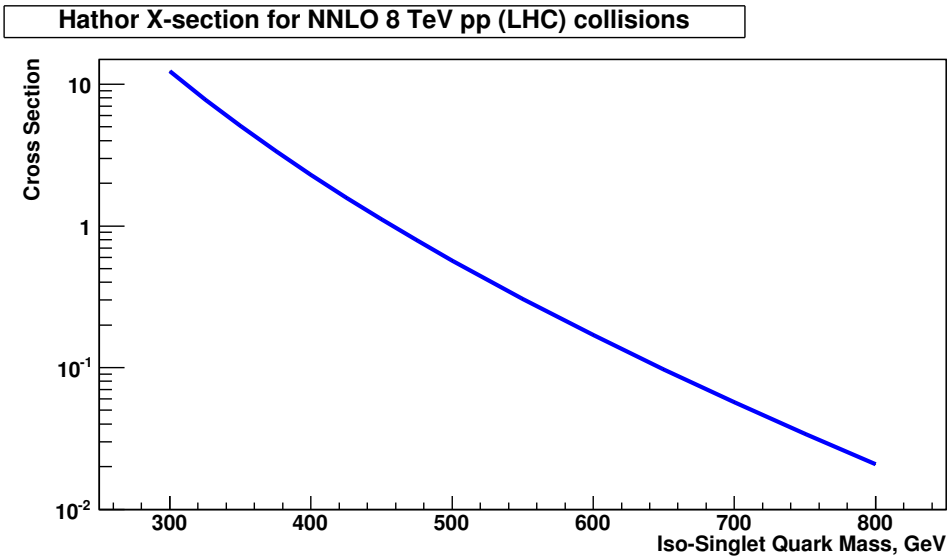

Figure 2.3. Hathor X-section For NNLO 8 TeV pp (LHC) Collisions.

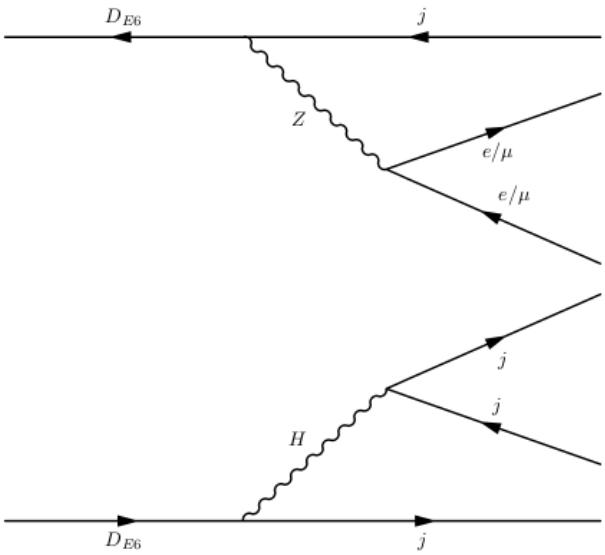

Figure 2.4. Iso-Singlet Quark Decaying Into The H-Z Channel Z Boson Decaying Into The Leptonic Channel.

3. THE ATLAS EXPERIMENT

3.1. The LHC

The LHC stands for Large Hadron Collider, and it is 27 km circular particle collider that collides protons or lead ions. It resides at the border of France and Switzerland near Geneva, $50 - 175$ m beneath the ground, shielded from outside factors. It has been built by CERN between 1998 - 2008, designed to accelerate protons up to 7 TeV and lead ions to 574 TeV per nucleus (2.759 TeV per nucleon pair). To discover rare particles, LHC is designed to obtain a high luminosity. At full capacity, the luminosity is expected to be $L = 10^{34}\,\mathrm{cm}^{-2}\mathrm{s}^{-1}$ with 1.15×10^{11} protons per bunch, and 25 ns between bunches. It can accelerate beams both clock wise and counter clock wise simultaneously so that two beams can be to collided at four designated points where detectors are situated.

The LHC accelerates protons which have already been pre-accelerated by the LINAC2, Proton Synchrotron Booster(PSB), Proton Synchrotron(PS) and Super Proton Synchrotron(SPS). LINAC2 accelerates protons from its hydrogen source to 50 MeV , from there protons are accelerated to 1.4 GeV by PSB, 25 GeV by PS and 450 GeV by SPS. Finally protons are injected to LHC. Currently LHC can accelerate protons up to 4 TeV and collide them with a center of mass energy of 8 TeV.

The LHC houses 7 different experiments which are ATLAS, CMS, ALICE, LHCb, TOTEM, MoEDAL and LHCf. The first four of these experiments are located right at the four collusion points of the LHC. ATLAS and CMS experiments are multipurpose detectors designed for searching for new particles. ALICE is designed for researching gluon-gluon plasma obtained in heavy ion collusions in LHC and LHCb experiment concentrates on b-physics measuring the charge parity(CP) violation in bottom quark interactions.TOTEM experiment measures proton-proton cross section, MoDEAL searches for magnetic monopoles and LHCf detector exam-

ines neutral pions produced at a zero-degree collusion angle in order to understand interactions of cosmic rays with Earth's atmosphere.

Currently the LHC does not function at full capacity. Table 3.1 lists the LHC running parameters as they stood right before the maintenance shutdown that started in 2013.

Table 3.1. LHC Parameters As Of December 12, The Values Are Taken From The Reference: [11].

Time Between Bunches	50 ns
Protons per Bunch	1.6×10^{11}
Number of Bunches	1374
Beam Energy	4 TeV
Peak Luminosity	7.7×10^{33}
Max. Number of Events per Bunch Crossing	40

3.2. The ATLAS Detector

ATLAS detector is a multipurpose particle detector with capabilities to detect massive high energy particles. It aims to discover new particles and prove or rule out beyond-the-standard–model physics theories. It is a cylindrical detector with the interaction point at its center. It has a layered structure with the inner detector surrounding the interaction point, and preforming charged-particle tracking with the help of the solenoid magnets. On the outer layers lie the calorimeters, the toroid magnets and the muon detector. Its overall structure can be viewed on figure 3.1.

3.2.1. The Coordinate System

The ATLAS detector's coordinate system takes the interaction point as the origin. The beam direction is taken as the z axis, positive x axis is directed at the

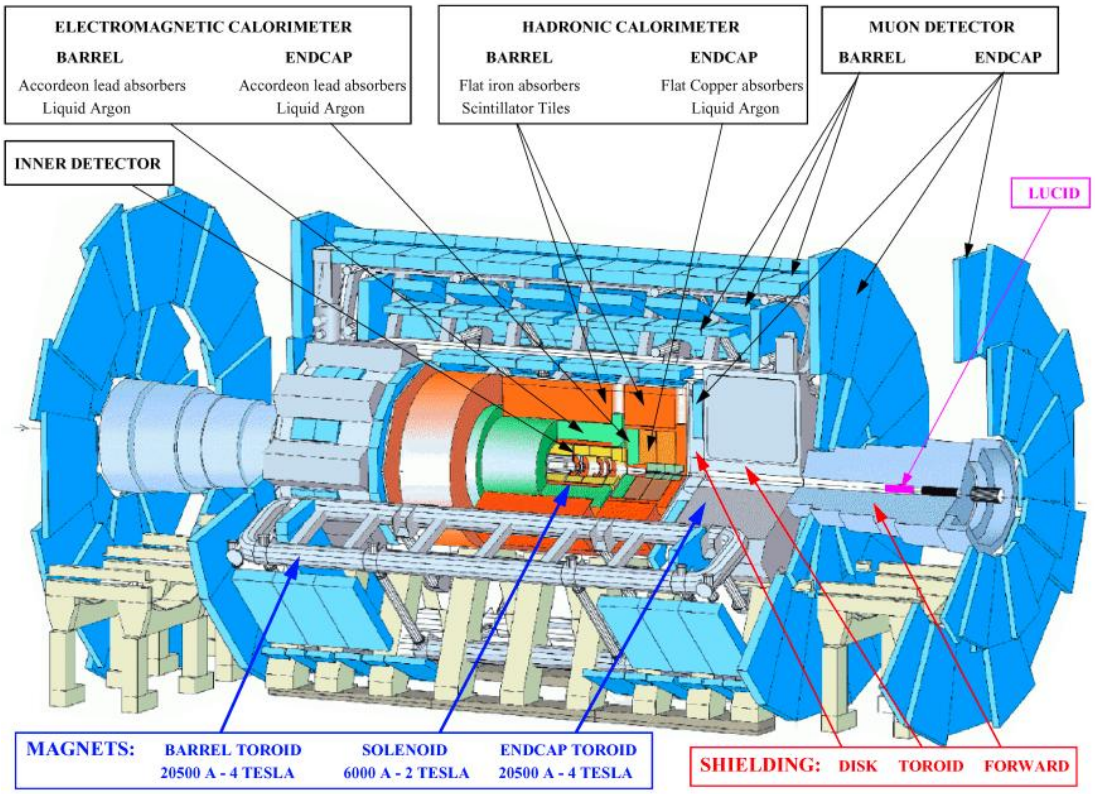

Figure 3.1. Overall View Of The ATLAS Detector, Taken From The Website [2].

center of the LHC ring and positive y axis points towards the sky. The transverse momentum p_T , transverse energy E_T and missing transverse energy E_T^{miss} and all transverse variables are defined on the $x-y$ plane. On the $x-y$ plane lies the azimuthal angle ϕ defined as $\phi = \tan^{-1} p_y/p_x$. Polar angle θ is defined with respect to the beam axis as $\theta = \cot^{-1} p_z/p_T$. Pseudo-rapidity η is defined as $\eta = -\ln(\tan(\theta/2))$.

3.2.2. Magnetic System

ATLAS detector has two different magnets: The solenoid magnet providing magnetic field for the inner detector and the toroid magnet providing magnetic field for the muon system.

The solenoid magnet is a compact, superconducting magnet which lie outside the inner detector before calorimeters. Its job is to provide a magnetic field for the inner tracker to identify charged particles and measure their transverse momenta. Solenoid

magnet provides a central magnetic field of 2 T along the z axis. Unlike the standard detector design where the magnets are placed outside the calorimeter, the solenoid magnet is located outside the inner detector before the calorimeter. This design prevents the magnetic field from spreading the showered particles in the calorimeter (better resolution), but on the other hand this design can cause the particles to start showering before they reach the calorimeter, while the solenoid acts as a material barrier between the inner detector and the calorimeter.

The toroid magnet system is composed of three subsystems. (the barrel and the two endcaps) The system has been designed to bend the trajectories of muons in order to allow the calculation of their transverse momenta. Each system consists of 8 superconducting coils stationed radially around the beam axis. The barrel system surrounds the electromagnetic calorimeter while the end cap systems are stationed at the both ends of the cylindrical shaped electromagnetic calorimeter. The three section toroid system can deliver a magnetic field of 3.9 T at the central region and 4.1 T at the end regions.

3.2.3. ATLAS Inner Detector

ATLAS inner detector is the innermost part of the ATLAS detector. Its objective is to track the charged particles which are bent by the solenoid magnets in order to measure the momenta and the trajectory of the charged particles. Its comprised of three main segments which are the pixel detector, semi-conductor detector and the transition radiation tracker.

3.2.3.1. Pixel Detector. ATLAS pixel detector is designed in order to work really close to the beam line providing high resolution to an order where it would be able to track individual particles inside a jet. They are especially useful in b-hadron reconstruction. The inner most layer of the pixel detector is called as the b-layer, and it functions to detect the secondary vertex for the b-hadrons. The detector is separated into three barrels with radii of 5 cm, 9 cm and 12 cm covering the beam line

cylindrically and three discs on each end cap, where discs are perpendicular to z axis. The detector is covered with 1744 silicon strips with each containing 46080 pixels.

3.2.3.2. Semi-Conductor Detector/Tracker (SCT). The SCT makes 8 precision measurements per track in the intermediate radial range. The SCT is composed of 4 barrel layers and 9 end-cap discs. Each layer itself comprised of two sub-layers which have micro-strip detectors placed with a small stereo angle. This provides both ϕ and z measurements. silicon strips detectors are single sided p-on-n semiconductor detectors which are radiation resistant and are activated even for minimum ionizing particles. Approximately 6.3 million channels are readout from the SCT.

3.2.3.3. Transition Radiation Tracker (TRT). The TRT detector is constructed using straw detectors. A straw detector is a small cylindrical detector with a wire passing through its z axis. The wire and the outer surface of the cylinder is oppositely charged creating a constant electric field. The cylinder is filled with a gas that ionizes as a charged particle passes through. The created ion pairs are then collected by either the wire or the outer shell of the detector. The TRT detector's barrel part contains about 50 k straws which can reach out to 1.44 m in length. The end-caps contain 320 k radial straws. Each straw gives a resolution of 170μ m and has two different energy thresholds. Using these two different thresholds the detector is able to discriminate between tracking and transition radiation hits which is used in electron identification, as electrons have significantly larger γ factors compared to heavier particles.

3.2.4. Calorimeters

Like most of the other high energy particle detectors, the ATLAS calorimeter also has electromagnetic and hadronic calorimeters. As their name suggest electromagnetic calorimeters are used for measuring the energy of electron and photon signatures while hadronic calorimeters are used for measuring the energy of hadron signatures. All of ATLAS calorimeters are sampling calorimeters.

3.2.4.1. Electromagnetic Calorimeter. When electrons or photons passes through dense material they start making showers. The physics behind these showers are well understood with a clean signature that can differ them from other sources of radiation. ATLAS detector's EM calorimeter is a lead liquid-argon detector with the range of $|\eta| < 3,2$ separated into a barrel part and two end caps.

As seen in figure:3.2 the EM calorimeter has accordion-shaped kapton electrodes and lead absorber plates. The lead plates facilitate the shower, creating charged pairs which ionizes the liquid argon. The ionized particles are then collected by electrodes. In the $|\eta| < 2.5$ region the EM calorimeter has 4 layers to increase sensitivity on both high and low energy particles.

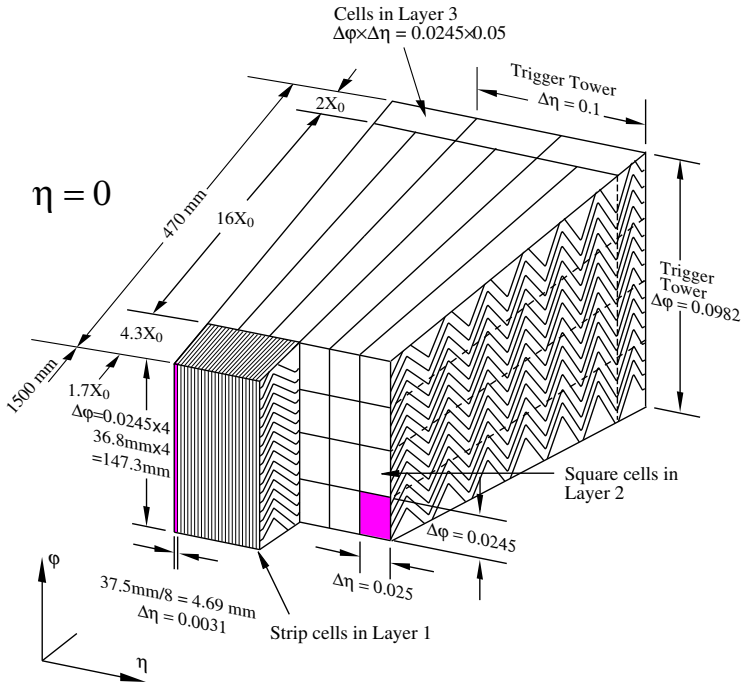

Figure 3.2. Cross Section Of The ATLAS Electromagnetic Calorimeter, Taken From The Website [2].

3.2.4.2. Hadronic Calorimeter. The hadronic showers are much more energetic and penetrative compared to the electromagnetic showers. For this reason hadronic calorimeter is designed in a way that it is able to stop the hadronic showers from reaching the muon detector. ATLAS's hadronic calorimeter is composed of tile and liquid Argon(LAr) calorimeters covering the $|\eta| < 4.9$ range.

The tile calorimeter system lies on the barrel region of the calorimeter system. It is made out of scintillating tiles and a steel matrix. The steel matrix is used as an absorber and the tiles are placed parallel to the $x - y$ axis to improve the e/h ratio.

Hadronic LAr calorimeter lies on both end-caps of the calorimeter. The difference of this LAr calorimeter to the EM calorimeter is that calorimeter uses copper as absorber plates in order to compensate for the increased radiation of the end-caps.

3.2.4.3. Forward Calorimeter (FCal). In addition to the EM and hadronic liquid Argon (LAr) calorimeters there exist the forward calorimeter which is also an LAr calorimeter. It is located inside the end-cap cryostat, covering the region of $3.1 < |\eta| < 4.4$ It is made out of three layers: the first layers, a Cu/LAr for electromagnetic measurements and two layers of W/LAr for hadronic calorimeters. FCal has a high stopping power with brass absorbers located directly behind FCal in order to prevent high energy hadronic showers reaching the muon detector.

3.2.5. Muon System

Muon system is the outer most part of the ATLAS detector. Muons are used both for event triggering and reconstruction. Since muons have high penetrative powers, the muon system covers the outer region of the ATLAS detector. The muon system is composed of four detectors of different technology which are the Monitored Drift Tubes (MDT), Cathode Strip Chambers (CSC) , Resistive Plate Chambers (RPC) and Thin Gap Chambers (TGC).

3.2.5.1. Monitored Drift Tubes (MDT). MDT lies in the $|\eta| < 2$ range. It is composed of tubes with 15 mm radius and length varying between 70 cm to 630 cm filled with Argon and CO_2. The tubes are layered on top of each other with 3-4 layers depending on location and 2 of such bunches are set parallel to each other with a gap in between that allows the muons to drift. The MDT structure can be viewed on the

figures: 3.3 and 3.4.

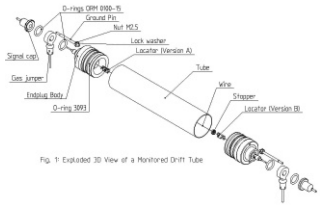

Figure 3.3. Single Tube of MDT Detector, The Image Is Taken From The Website [2].

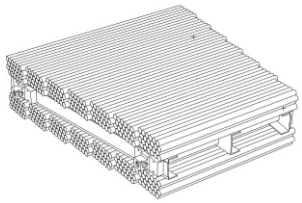

Figure 3.4. General MDT Structure, The Image Is Taken From The Website [2].

3.2.5.2. Cathode Strip Chambers (CSC). CSC is the second part of the muon tracking system. It covers the range of $2 < |\eta| < 2.7$ replacing the MDT in the forward regions. CSC is made out of multi wire proportional chambers with $2.5mm$ wire spacing. The cathode and anode wires are perpendicular giving resolution in two dimensions.

3.2.5.3. Resistive Plate Chambers (RPC). Resistive Plate Chambers are used for triggering purposes. They cover the range of $|\eta| < 1.05$ and they are made out of two charged parallel plates with gas filled filling the gap. They have 1 ns time resolution and have dimensional resolution of 1 cm on all planes allowing fast responses for triggering.

3.2.5.4. Thin Gap Chambers (TGC). Similar to CSC, TGC replaces the RPC system on the forward range of the detector covering the range of $1.05 < \eta < 2.4$. It is the second part of the triggering system and its structure is similar to the MDT chambers with the difference of anode wires having larger pitch then the anode-cathode distance. It has a gas mixture of CO_2 and $n-$pentane. Similar to the RPC it has a small resolution time making it suitable for triggering events.

3.3. Trigger And Data Acquisition (TDAQ)

LHC's bunch crossing frequency is 40 MHz and the ATLAS detector can store events permanently at a rate of about 100Hz on average. Hence the detector has been designed such that it selects and stores the events that are physically interesting and rejects the data from most of the collisions. The system responsible for this selections is called the TDAQ system. The TDAQ system is responsible for performing its task with absolute minimum bias for actual physics studies. The subsystem responsible for this selection is called the trigger.

ATLAS's trigger system is composed of 3 stages. Level 1 Trigger is the hardware trigger that reads data from the muon system and the calorimeters. Large energy deposits inside the calorimeters and hits from the TRC, RPCs are analyzed. The trigger is designed to make a decision on an event in 2.5μ s with an output rate of 75 kHz . The safety of information on this level trigger is secured by using a pipeline memory and recalling events from the memory.

Level 2 Trigger is a software trigger. As Level 1 makes its decision, the chosen events are stored in the read out buffers (ROBs). Level 2 Trigger accesses the information from the ROBs and improves on level 1 trigger requirements by using data from all of the sub-detectors (including the inner detector) at full granularity, but only in regions of interest identified by the level 1 trigger. Level 2 trigger's output rate is about 1 kHz.

Level 3 Trigger also called event filter. It is a software trigger. Full event data is available at this trigger, and object recognition can be performed using essentially the off-line reconstruction algorithms.The output rate is reduced to 100Hz which is a rate that the ATLAS data storage system can handle.

4. OBJECT RECONSTRUCTION AT ATLAS

After the event selection of the ATLAS detector, the information from the different detectors are put together and objects are reconstructed. This is done off-line via reconstruction algorithms. At the end of this process, particles are identified with their four momentum, charge, tracks , primary vertex and flavor. Reconstruction algorithms vary according to the signal/particle and needs to be examined separately.

4.1. Track Reconstruction

As charged particles pass through the inner detector, they leave tracks. These tracks carry vital information for object reconstruction and momentum measurements. Each track is identified by five variables.

- η and ϕ: The direction of the track in terms of its polar and azimuthal angles.
- d_0 and z_0 : The transverse and longitudinal distance between the track and the beam axis at the point of closest approach
- charge $\times 1/P_T$: The signed inverse transverse momentum of the particles calculated by the bending of magnetic field.

To measure these variables, there are various algorithms used [12]. The baseline algorithm is the inside-out algorithm. It starts from 3-point seeds in the silicon detectors adding more hits along its way till the TRT using a Kalman filter. This method is used for primary particles with $P_T > 400\,\mathrm{MeV}$. In addition to the inside-out algorithm there is an inverse method of back-tracking where the tracks are originated from the TRT extending them inwards following the silicon hits.

4.2. Vertex Reconstruction

As is customary for collider experiments, the vertices in the ATLAS detector are grouped in to two categories. The primary vertices (PV) correspond to the point where the collusions occurred and the secondary vertices correspond to the particle decays. The location of PVs are reconstructed using an iterative vertex finding algorithm. [12] The algorithm works by making a χ^2 fit using the seed and near by tracks. Each track is given a weight and according to this weight tracks incompatible with vertex by 7σ are used as a new vertex seed. Each vertex is required to contain at least 3 tracks for robustness. The vertex with with the largest sum of track squared momenta is chosen as the PV or the hard interaction.

4.3. Electrons

4.3.1. Electron Reconstruction

In ATLAS the electrons' energies are deposited inside the EM calorimeter. In order to reconstruct electrons, the EM clusters (deposits in the EM calorimeter) with an energy signature over 2.5 GeV and size of 3x5 middle layer cell unit hits are searched with a sliding-window algorithm. If a cluster is matched with a track originated from a photon vertex, it is tagged as a photon on the other hand if it is matched with another ID track, it is tagged as an electron candidate. From Monte Carlo simulations the algorithm has an expected efficiency of %95 at $E_T = 5\,\text{GeV}$ and 100% efficiency for $E_T = 15\,\text{GeV}$ from the electrons that originate from W and Z decays [13].

Electron energy is calculated using the deposited energy in the cluster and the energy is corrected for bremsstrahlung effects by adding several tracks together in a certain ΔR if necessary.

4.3.2. Electron Identification

Since electrons do not leave any signatures in the hadronic calorimeter and their cluster size is smaller than hadrons, the electron signal can be differed from hadrons. The real challenge lies in distinguishing π^0 and η mesons from electrons. The decay of these mesons to photon pairs creates two close showers on the EM calorimeter forming an electron like signature on the 2nd layer EM calorimeter. To separate these mesons from electrons, the innermost layer of the EM calorimeter is used.

There are various cuts applied to particles that are identified as electrons in order to separate them from jets. Depending on these cuts, electrons are given different identification tags. In this analysis the electrons that are tagged as *medium* and *tight* are used for electron identification. Tight electron selection is successfully able to reconstruct $\sim 70\%$ of the electrons while stressfully removing the background [14]. Tight tagged electrons are used in the analysis. The medium are used for estimating the QCD background.

- Medium: The electrons with this tag lies in the $|\eta| < 2.47$ range excluding the $1.37 < |\eta| < 1.52$ zone where there is a transition region between the barrel and the end cap EM calorimeters. They should have a minimum transverse energy of $E_T > 25\,\text{GeV}$ and with $z_0 < 2\,\text{mm}$. They should be identified with a certain shower shape and must have at least 1 hit in the first pixel layer and at least 7 hits in total on the SCT and pixel detectors. In addition, overlap removal between muons/jets and electrons are done.
- Tight: In addition medium requirements, tight tagged electrons are expected to have a distance $|\Delta\phi| < 0.02$ and $|\Delta\eta| < 0.005$ between the cluster and the track. The tracks should also be isolated around a region of E_T cone of $R = 0.2$ centered around the electron and P_T cone of $R = 0.3$.

4.3.3. Electron Corrections and Scale Factors

While Geant4 detector simulation is quite accurate, there are still some discrepancies between the generated Monte Carlo(MC) samples and data. To account for these discrepancies, scale factors are applied to electron samples. These include scale factors to handle the discrepancies in reconstruction, trigger and isolation cut efficiencies. Furthermore, energies of electrons in the MC samples are smeared to match the energy resolutions observed in data.

4.4. Muons

4.4.1. Muon Reconstruction

The muon reconstruction is done using the signals from the muon spectrometer, the inner detector and the calorimeter. There are four different muon reconstruction methods which are summarized below. [15] Amongst these, the combined muon candidates have the highest correct identification rate but the performance varies according to the location of the trajectory of the muon.

- Stand-Alone Muons: The muon energy and trajectory is measured using data only from the muon spectrometer. The track is reconstructed using the hits in the muon system (MS) and the point of the the track closest to the beam line.
- Combined Muons: Tracks are separately reconstructed in the ID and the MS. When an ID and a MS track can be matched, they are combined in order to obtain the track of the muon.
- Segment-Tagged Muons: If a track found in the ID is associated with a track segment from MDT or CSC, it is identified as a Segmented-tagged Muon.
- Calorimeter-tagged Muons: ID tracks are matched with calorimeter deposits that show muon signatures. This method is generally used for the region $\eta \approx 0$.

4.4.2. Muon Identification

Compared to electrons, the muons are less likely to be misidentified as jets or other objects but still there are some criteria to purify the muon samples. In this thesis two tags for muons are used. Tight tagged muons are used for event reconstruction while the medium tagged muons are used for estimating the QCD background.

- Medium: The muon is required to have been reconstructed with combined muons method, with $P_T > 25\,\text{GeV}$, $|\eta| < 2.5$ and $|z_0| < 2\,\text{mm}$. It should have at least 1 b-layer hit in the pixel detector, at least 5 SCT hits and at least 5 TRT hits in the $0.1 < |\eta| < 1.9$ region. In addition, overlap removal between jets and muons are performed.
- Tght: In addition to all the medium requirements, there is an isolation cut which requires P_T cone $/P_T < 0.005$.

4.4.3. Muon Corrections and Scale Factors

Similar to electrons, scale factors are applied to the MC samples to account for discrepancies of MC with data. For muons, these are the reconstruction and trigger efficiency scale factors. Moreover, the momenta of the muons are smeared to get the MC to agree with momentum resolution in data.

4.5. Jets

When a large number of particles have smaller relative momentum with respect to each other than their own transverse momenta in the lab frame, they cluster together into a small cone inside the detector. Such sets of particles are called jets. In general jets are associated with an initial high-momentum parent particle and in ATLAS this is quite often a gluon or a quark. (Though in occasion it can also be a heavy particle such as a vector boson).

4.5.1. Jet reconstruction

Jets are reconstructed using the anti-k_t algorithm [16]. The anti-k_t algorithm works in the following manner: Among the particles that could belong to a jet, the ones that have the highest P_T are selected. Then all particles within a cone of radius R around the high P_T particles are bunched together to from a jet cluster . If two of such clusters coincides in the same region, depending on their distances, the two jet clusters are either combined or designated as two separate jet clusters. This method is sensitive in finding the high P_T jets but is insensitive for finding the low P_T jets which are insignificant in this analysis. [17] Currently in ATLAS the $R = 0.4$ [16].

4.5.2. Jet Energy Calibration

In ATLAS while reconstructing jets, energy looses could occur while there are insensitive locations in the detector, there are particle leakages out of the calorimeter, particles at low momenta are missed by the reconstruction algorithm, the particles from a different source can be associated with the wrong jet or there could be other unlisted issues as well. In order to compensate these loses there, are various methods. In this analysis local cluster weighting and jet energy scaling method is used.

- Local Cluster Weighting (LCW) and Jet Energy Scaling (JES): This is a Monte Carlo based algorithm. It uses the Energy density, isolation and penetration depth inside the calorimeter and similar cluster properties in order to calibrate the clusters individually. After each cluster is calibrated, the energy of the jet is reconstructed. After the reconstruction a final scale factor is applied on the jets.

4.5.3. Jet Identification

In this analysis, tight requirements are used for jet identification. All jets are required to have $P_T > 25\,\text{GeV}$ and $|\eta| < 2.5$. In addition to this, to reduce the

effect of pile-up, jets with $P_T < 50\,\text{GeV}$, $|\eta| < 2.4$ and $|JVF| < 0.5$ are removed (Jet vertex fraction(JVF) is defined as the probability that the jet is originated from its associated vertex). Also overlap removal between muons and electrons are done in order to minimize the misidentification rate.

4.5.4. B-Tagging

According to the SM a Higgs boson at 125GeV is expected to decay into a b-quark pair $\approx 60\%$ of the time. For this reason b-quark identification becomes a strong tool in this analysis to correctly reconstruct the Higgs boson. The life time of the b-quark is comparably longer then most of the other quarks, jets originating from the b quarks can be separated from other jets by using the presence of a secondary vertex in the jet and its distance to the primary vertex. In this analysis MV1 tagger is used for b-tagging which generates a b-tagging weight for the jets using a neural network algorithm. We identify the b-jets using a cut on this variable. The efficiency of this cut is 70% on actual b jets from $t\bar{t}$ events.

5. E_6 ISO-SINGLET QUARK SEARCH IN HIGSS, Z CHANNEL

5.1. Event Selection and Reconstruction

Event selection and reconstruction are what make an analysis unique. The focus of this chapter will be the selection and reconstruction algorithm of $D\bar{D}$ events in the H+Z channel. On tables 5.2 and 5.3 the event selection and reconstruction flow and their efficiencies can be found.

5.1.1. Event Selection

The event selection algorithm uses the objects that are reconstructed according to the criteria in Section 4. The event selection criteria themselves can be classified under two broad groups. The first type is meant to remove the low quality data from the analysis. The second type is designed to remove the background events in order to boost the signal significance.

5.1.1.1. Removal of Low-Quality Data. ATLAS detector cannot work flawlessly, for this reason various cleaning cuts needs to be applied to the events. These set of cuts also remove the events with conflicting object identification and events from cosmic rays. All of these cuts are recommended by the ATLAS collaboration for the top quark analyses, which are similar to this analysis .

- Good Run List Cut (GRL Cut): The ATLAS collaboration periodically checks and tags the events which are suitable for analysis. The detector and collider conditions during data taking are not assessed on an event-by-event basis, but instead for short chucks of data called luminosity blocks(LB). Hence the LB consists the atomic unit of the ATLAS data and those LBs that are found good for a particular set of data analysis are put on to the GRL. We use the data in

the GRL recommended for top-quark analysis The integrated luminosity for the data used in this thesis is measured for events in the GRL.

- LAr Error Cut: During operation the liquid Argon calorimeter (LAr) system can occasionally malfunction and send burst signals in many isolated cells in the form of distorted pulses. The events that are tagged/associated with these pulses are removed from the analysis.
- Incomplete Event Cut: The events which have missing information and are flagged as incomplete are removed for the analysis.
- Tile Trip Cut: In addition to LAr bursts, the readout cells of the LAr detector may also trip and cause information loss. Events with such trips are removed from the analysis.
- Cosmic Event Rejection: Although unlikely, cosmic muons can penetrate the ATLAS detector resulting in two back-to-back muon signals . To remove these events we use their d_0 (transverse impact parameter) values. If two muons pairs have the same sign d_0 value where $d_0 > 0.5$, then the $\Delta\phi$ difference between their azimuthal angles is calculated and if $\Delta\phi > 3.10$, the event is tagged as a cosmic event and is rejected from the analysis.
- e-μ overlap: The events where an electron is located within a certain ΔR of a muon,are removed since the lepton has a chance of being miss tagged.
- Bad Jets Cut: If there are any jets that are tagged as a bad jet the event is dropped. A bad jet is a loose jet definition.

5.1.1.2. Background Event Removal. LHC being a hadron collider, the analysis relies on the leptonic Z Reconstruction for background removal. The lepton related cuts are the trigger cuts, lepton number cut, charge cut and the Z window requirement. In addition to the lepton related cuts, the analysis requires 4 jets to reconstruct the Higgs boson and the E_6 iso-singlet quarks. The combination of the lepton cuts and the 4 jet cut forms the backbone of the background rejection. The detailed cut flow is as follows.

- Event Trigger: Since the analysis is run separately on electrons and muons, this cut only allows the events that are triggered by the correct lepton type to continue with the analysis.
- $\#_{vtx} >= 5$: Given that many particles (including 4 jets) are present in the signature events, the primary vertex is expected to have many tracks associated with it. So the main primary vertex (which has been selected as the one with highest sum P_T) is required to have at least 5 tracks.
- Exactly Two Leptons: The events that contain exactly 2 leptons (e or μ) are chosen, the rest of the events are removed. The leptons are required to share the same flavor and they should also share the same flavor as the trigger.
- Lepton Trigger Match: The events are expected to be triggered by one of the two leptons that has been observed. This cut removes the events in which one of the existing leptons is not the source of the trigger.
- At least 4 Jets: In this analysis the signal requires at least 4 jets so the event can be reconstructed. Removing events with fever then 4 jets reduces the background significantly.
- Opposite Signed Leptons: Since the analysis reconstructs a Z boson out of 2 leptons, the leptons are expected to have opposite charges. The events that contain same charge lepton pairs are removed.
- Z Window Cut: The ATLAS detector's Z boson mass resolution is really sharp, for this reason a tight Z Window is applied to remove the background. According to the MC signal analysis, this resolution is $\sim 2\,\text{GeV}$ for $Z \to ee$ and $\sim 3\,\text{GeV}$ for $Z \to \mu\mu$ For this analysis the Z window is chosen to be 5 times the resolution. So for electrons(muons) $|m_{e^+e^-} - m_Z| > 10(15)\,\text{GeV}$ is required.

5.1.2. Event Reconstruction

The event reconstruction is the heart of the E_6 analysis. In the analysis the Z reconstruction is simply done by combining the two opposite charge leptons that are left after the cuts. The real challenge lies in selecting the jets for the analysis, this is done via a χ^2 algorithm, which runs on all jet combinations in order to choose

the best possible candidates for Higgs and E_6 iso-singlet reconstruction. The further details of the χ^2 algorithm can be found in Section 5.1.2.1

The current E_6 analysis actually runs three χ^2's together. The differences of each of these χ^2 is the b-tagging condition of the Higgs boson. The first analysis doesn't force any b-tagging on the Higgs boson, the second analysis requires at least 1 b-tagged jet and the third and final analysis requires exactly two b-tagged jets to reconstruct the Higgs Boson. The χ^2algorithm is run thrice, one for each case. In this analysis if b-tagging is not required then a significant feed through can be expected from various E_6 decay channels that contains a Z boson into our analysis like Z+Z or Z+W channels. When a b-tagging is forced on the jets from the Higgs boson, the feedthrough is greatly reduced and this requirement also reduces background. When both jets that reconstructs the Higgs boson are required to be b-tagged, this greatly reduces the background, but at a major cost on the signal efficiency.

5.1.2.1. The χ^2 Algorithm. The χ^2 algorithm in essence is a simple algorithm. Each jet combination is assigned a weight according to its resemblance to the E_6 signal. The jet combination that minimizes this weight is also chosen to reconstruct the E_6 signal. In addition to weighting, the χ^2 algorithm is used for applying additional cuts on the jet combination. These cuts are b-tag cut on the jets associated with the Higgs boson and the minimum P_T requirement of the prompt jet.

Starting with the Higgs reconstruction, two jets are selected among the jets. According to the b-tagging requirements of this analysis the jet combination is either accepted or rejected. If they are accepted then the two jet momenta are combined using a 4-vector summation. The combination's invariant mass forms a candidate Higgs Mass denoted as m^{reco}_{Higgs}. Using this m^{reco}_{Higgs} , and the nominal mass of the Higgs which is denoted as m^{real}_{Higgs} the following Equation 5.1 , χ^2_{Higgs} is computed. σ_H stands for the reconstructed width (resolution+natural width) of the Higgs boson

mass which is to be determined later in Section 5.1.3.

$$\frac{(m_{Higgs}^{reco})^2 - (m_{Higgs}^{real})^2}{\sigma_H^2} = \chi_{Higgs}^2 \tag{5.1}$$

After Higgs reconstruction, the reconstruction of the E_6 iso-singlet quarks begins. This part of the χ^2 algorithm is meant to facilitate the selection of jets that creates two heavy quarks, the difference whose masses are minimal. Two previously unassigned jets are selected, and their P_T values are checked. It is expected that at least one of these jets, which are denoted as prompt jets, have $P_T > 100\,\text{GeV}$. This requirement is introduced as the E_6 quarks are expected to have a mass of 250 GeV or higher and their decay products should have high P_T. The 100 GeV value was set conservatively assuming an E_6 quark mass of 300 GeV. If none of the jets satisfy this requirement, a new jet combination is chosen. If it is satisfied then one of the jets is combined with the reconstructed Z boson forming the one D quark with mass $m_{D_Z}^{reco}$ and the other jet is combined with the reconstructed Higgs boson candidate forming the another D quark, with the mass $M_{D_Z}^{reco}$. Then a χ^2 value is calculated using the following Equation 5.2. In this equation σ_{D_Z} (σ_{D_H}) is the reconstructed width of the D_Z (D_H) quark.

$$\frac{(m_{D_Z}^{reco} - m_{D_H}^{reco})^2}{(\sigma_{D_Z})^2 + (\sigma_{D_H})^2} = \chi_{E_6}^2 \tag{5.2}$$

After calculating the $\chi_{E_6}^2$ and χ_{Higgs}^2 , they added together and stored. These two values are calculated for all jet combinations as long as they satisfy the jet P_T and b-tagging requirements. The jet combination that minimizes the summation of these two values is selected as the final jet selection. If the minimum total χ^2 value is higher then 15, then the event it self is dropped. The same stands for cases where no jet combination satisfies the jet P_T and b-tagging requirements.

5.1.3. Derivation of Event Selection/Reconstruction Parameters

In order for the event selection and reconstruction to function properly, the event selection and reconstruction parameters should be set properly. The only event selection parameter is the size of the Z mass window. The event reconstruction parameters are the minimum prompt jet P_T, maximum total χ^2 allowed, E_6 χ^2 errors ($\sigma_{D_Z^{reco}}$, $\sigma_{D_H^{reco}}$) and the Higgs χ^2 error σ_H. Each of these parameters should be selected in order to minimize the background and maximize the signal reconstruction efficiency. These variables are set according to an iso-singlet E_6 quark at a mass of 300 GeV, which is expected to give be compatible results for heavier iso-singlet quarks as well. The complete list of the set parameters can be found on the Table 5.1

Table 5.1. Values Set For The Parameters Used In This Analysis.

Parameters	**Electron Channel**	**Muon Channel**
Z Window Range	$\pm$10 GeV	$\pm$15 GeV
σ_H **Variable**	12 GeV	15 GeV
Prompt Jet P_T **Variable**	100 GeV	100 GeV
σ_{D_Z} **Variable**	25 GeV	30 GeV
σ_{D_H} **Variable**	45 GeV	40 GeV
Maximum Allowed χ^2	15	15

5.1.3.1. Z Window Range. The Z window variable holds a crucial importance on removing some of the major sources of the background from the analysis. The current Z window is set according to the reconstructed width of the Z boson in the 300 GeV E_6 signal sample. The figures 5.1 and 5.2 show the Z mass histograms of 300 GeV E_6 quark signal for both triggers. The Z shapes in both triggers are completely observed to be Gaussian with a small width. The width of the electron sample is about 2 GeV and the width pf the muon sample is about 3 GeV. In this analysis it is decided to set the Z window 5 times larger then width of the Z boson reconstructed from the signal MC. This decision ensures that the majority of the Z signals to reconstructed while still being able to reject a significant amount from the background. (The Z+jets

background composes the 90% of the overall background).

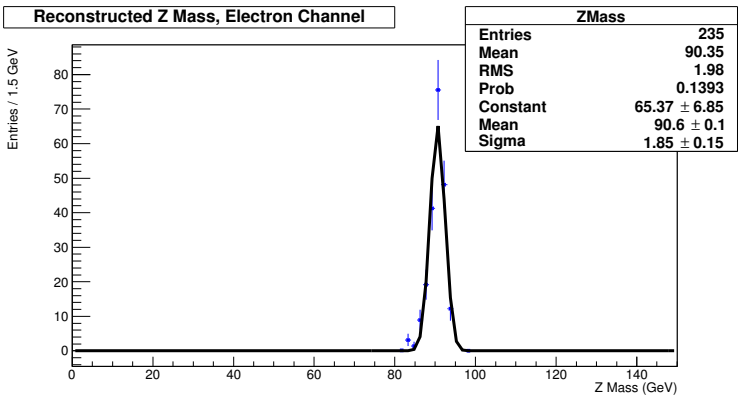

Figure 5.1. Reconstructed Z Mass Histogram From The 300 GeV Signal MC Sample In The Electron Channel.

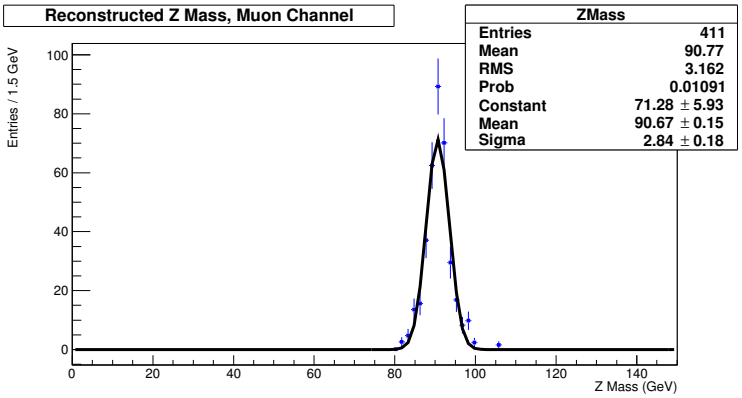

Figure 5.2. Reconstructed Z Mass Histogram From The 300 GeV Signal MC Sample In The Muon Channel.

5.1.3.2. σ_H Parameter. This parameter is set to the Gaussian width of the reconstructed Higgs mass histogram of the 300 GeV E_6 signal MC sample. The figures 5.3 and 5.4 show the Gaussian fit to the reconstructed Higgs mass for electron and muon channels. The Gaussian fit is again a good fit for the Higgs signal, although the effect of the χ^2 algorithm smoothening the Gaussian fit cannot be disregarded. (We apply a bootstrap method.) According these results, the electron channel's width is found to be ≈ 12 GeV and the muon channel's width is found to be ≈ 15 GeV.

5.1.3.3. Prompt Jet Minimum P_T Parameter. The E_6 heavy quark can also be distinguished from the known SM particles by the help of the fact that when it decays,

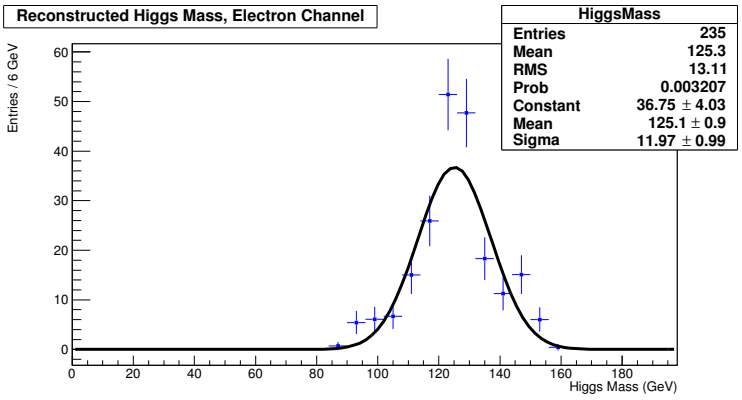

Figure 5.3. Reconstructed H Mass Histogram From The 300 GeV Signal MC Sample In The Electron Channel.

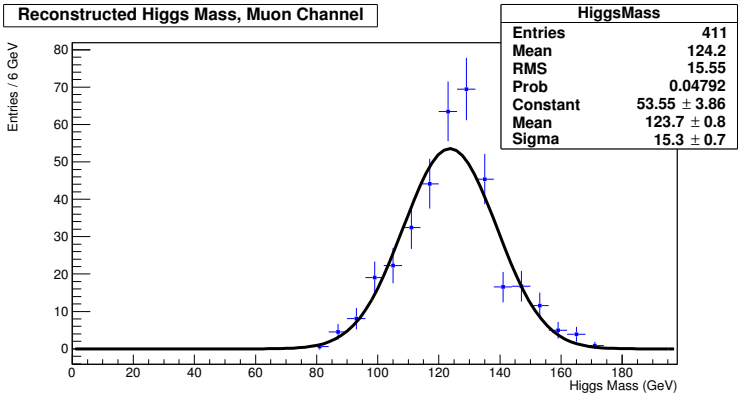

Figure 5.4. Reconstructed H Mass Histogram From The 300 GeV Signal MC Sample In The Muon Channel.

the daughters are expected to have high P_T. For this reason, asking one of the prompt jets to have P_T higher then a threshold value can improve background rejection and the correct jet assignment for the reconstruction efficiency of the iso-singlet quarks. To determine this threshold the E_6 signal's jet P_T histograms are analyzed. The leading jet P_T distribution can be found on the figures 5.5 and 5.6 . According to these figures putting a P_T cut around 100 GeV would have a minute effect on reducing the signal but could reduce the background significantly. As the E_6 quark mass increases, the P_T cut will become more conservative.

5.1.3.4. σ_{D_Z} and σ_{D_H} Parameters. Similar to the σ_H parameter, the σ_{D_Z} and σ_{D_H} parameters are obtained by Gaussian fit in the 300 GeV E_6 signal MC samples. This

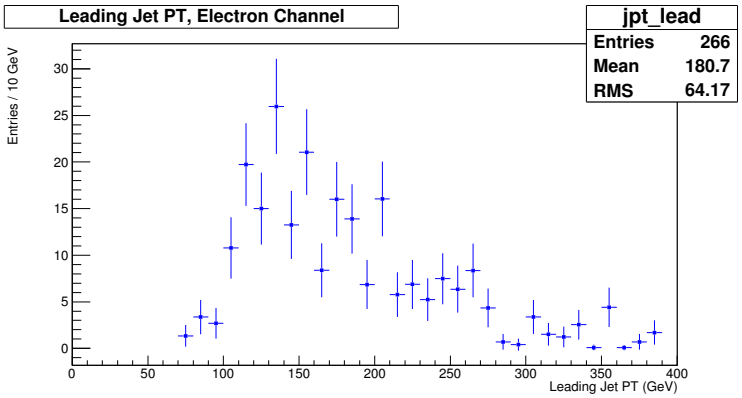

Figure 5.5. Leading Jet P_T Of The 300 GeV Signal MC Sample In The Electron Channel.

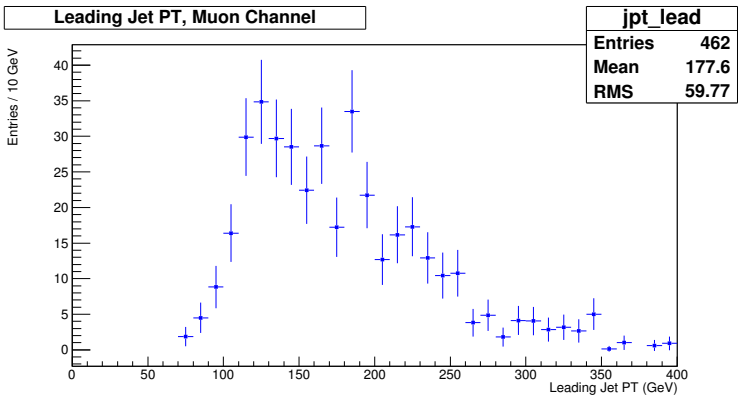

Figure 5.6. Leading Jet P_T Of The 300 GeV Signal MC Sample In The Muon Channel.

width range nearly stays constant with small variations as the E_6 signal's mass is swept . The figures 5.7 and 5.8 plots the width of the E_6 iso-singlet quark reconstructed from a Z boson. According to these figures, in the electron channel the width is 25 GeV and in the muon channel the width is 30 GeV. The second set of figures 5.9 and 5.10 plot the width of the E_6 iso-singlet quark reconstructed from a Higgs boson. According these figures, in the electron channel the width is 45 GeV and in the muon channel the width is 40 GeV. As it is visible, the Gaussian fit on these graphs are not perfect but they are decent enough to provide a benchmark value.

5.1.3.5. Maximum Allowed χ^2 Value . If the total χ^2 value is very high, one can conclude that either the Higgs reconstruction failed or the reconstructed E_6 quarks

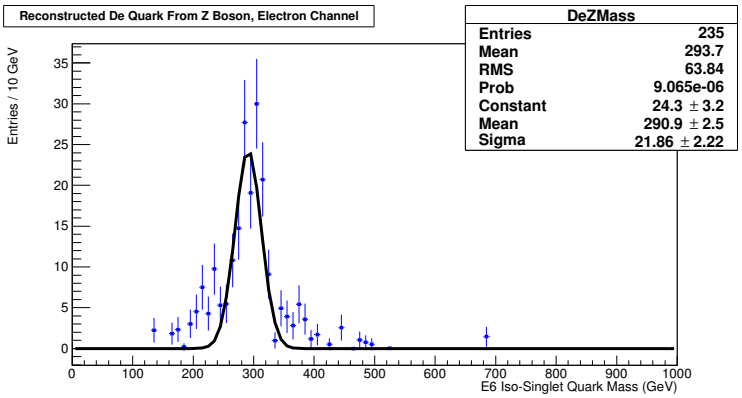

Figure 5.7. Reconstructed E_6 Iso-Singlet Quark From A Z Boson, Mass Histogram From The 300 GeV Signal MC Sample In The Electron Channel.

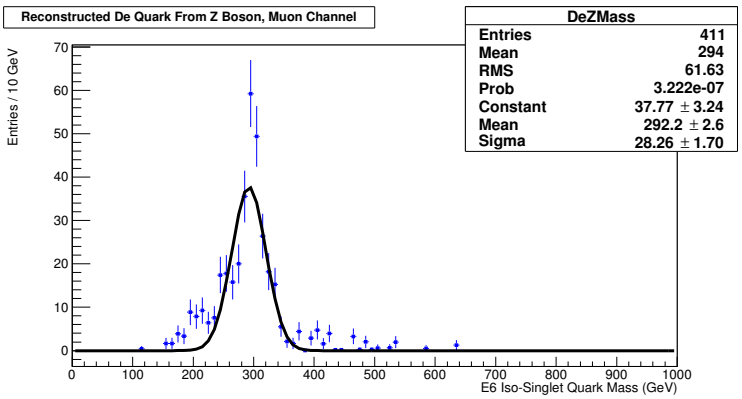

Figure 5.8. Reconstructed E_6 Iso-Singlet Quark From A Z Boson, Mass Histogram From The 300 GeV Signal MC Sample In The Muon Channel.

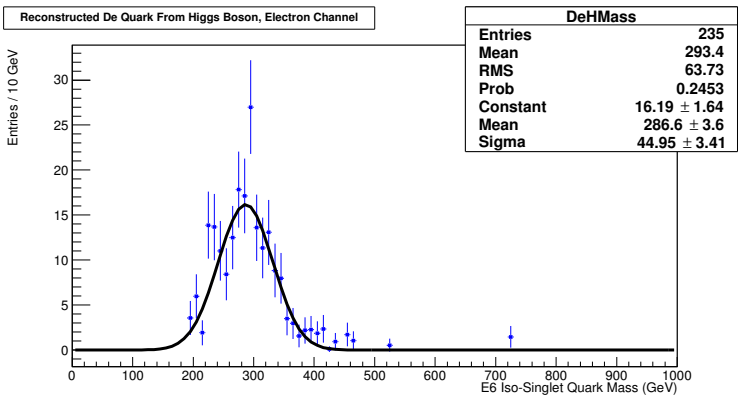

Figure 5.9. Reconstructed E_6 Iso-Singlet Quark From A Higgs Boson, Mass Histogram From The 300 GeV Signal MC Sample In The Electron Channel.

have a huge mass difference between them. If this is the case then it is illogical to accept these event since this means that we are accepting background events. For

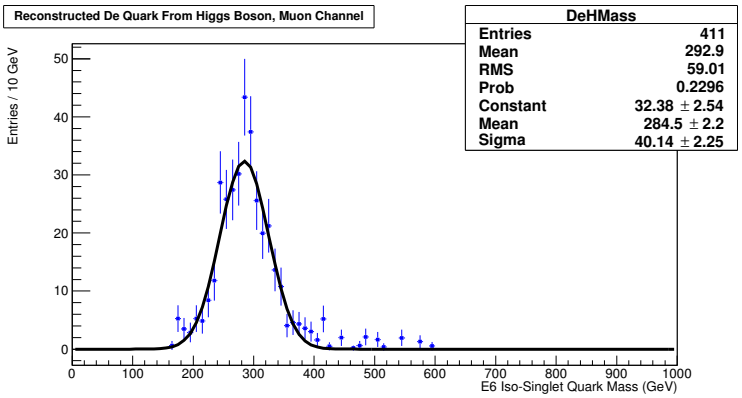

Figure 5.10. Reconstructed E_6 Iso-Singlet Quark From A Higgs Boson, Mass Histogram From The 300 GeV Signal MC Sample In The Muon Channel.

this reason there is an maximum allowed χ^2 value for the analysis. This value is set according to the χ^2 distribution of the E_6 signal at 300 GeV. The distribution can be found on the figure 5.11. In this figure only few events are able to cross a certain χ^2 value so putting cut around 15 doesn't reduce our signal but would reduce the background. As a side note, this χ^2 distribution was filled when the χ^2 cut was removed.

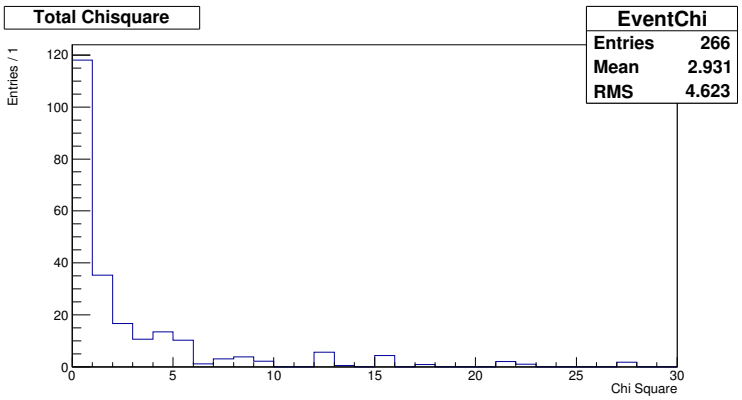

Figure 5.11. Total χ^2 Of Each Event (Signal Monte Carlo).

Table 5.2. Efficiency Table For The Muon Channel.

Cut Name	**Efficiency , 0 b-tag**	**Efficiency , 1 b-tag**	**Efficiency , 2 b-tag**
Inital	1	1	1
GRL	0.9555	0.9555	0.9555
Lar Error	0.9979	0.9979	0.9979
Tile Error	1	1	1
Incomplete Event	1	1	1
Tile Trip	1	1	1
Cosmic Event	1	1	1
Event Trigger (Muon)	0.5676	0.5676	0.5676
$\#_{vtx} >= 5$	0.9832	0.9832	0.9832
# Muons == 2	0.0356	0.036	0.0356
e-μ Overlap	1	1	1
Bad Tagged Jets	0.9988	0.9988	0.9988
# Jets == 4	0.0028	0.0028	0.0028
Opposite Signed Muons	0.9979	0.9979	0.9979
Z Window	0.7682	0.7682	0.7682
χ^2	0.3752	0.0677	0.0083
Overall Efficiency	0.001505 %	0.0002718 %	0.00003346 %

Table 5.3. Efficiency Table For The Electron Channel.

Cut Name	**Efficiency , 0 b-tag**	**Efficiency , 1 b-tag**	**Efficiency , 2 b-tag**
Inital	1	1	1
GRL	0.9577	0.9577	0.9577
Lar Error	0.9979	0.9979	0.9979
Tile Error	1	1	1
Incomplete Event	1	1	1
Tile Trip	1	1	1
Cosmic Event	1	1	1
Event Trigger (Electron)	0.7344	0.7344	0.7344
$\#_{vtx} >= 5$	0.9869	0.9869	0.9869
# Electrons == 2	0.01539	0.01539	0.01539
e-μ Overlap	1	1	1
Bad Tagged Jets	0.9989	0.9989	0.9989
# Jets == 4	0.002651	0.002651	0.002651
Opposite Signed Electrons	0.9841	0.9841	0.9841
Z Window	0.7215	0.7215	0.7215
χ^2	0.3596	0.05354	0.007202
Overall Efficiency	0.0007211 %	0.0001074 %	0.00001444 %

6. DATA, SIGNAL AND BACKGROUND

This section summarizes all the data and MC samples used in the analysis, and explains how a data-driven scale factor is computed for the Z+jet background MC. A summary of the section is available at Table 6.1 where all the MC samples are listed with their cross-sections.

6.1. Data

This analysis uses the data recorded by the ATLAS detector during its 8 TeV run. The data were taken when ATLAS was running under its nominal conditions. The data files are separated according to the periods which signify their recording date.

6.2. Simulated Background Samples / MC Samples

The search for iso-singlet quarks in the Z+Higgs channel requires a clean lepton pair signal that can be reconstructed back to a Z boson. Since the ATLAS detector has high Z reconstruction efficiency, most of the non-Z background can easily be removed. For this reason, the dominant background is the Z+jets background which contributes to 90% of the overall background. The second biggest contribution comes from the $t\bar{t}$ and di-boson backgrounds which together contributes to 9% of the total background. The rest of the background is composed of single-top, QCD and W+jets backgrounds, whose contributions are minimal.

6.2.1. Z+Jets Background

The Z+jets background is the dominant background. For this analysis two different Z+jets samples have been used. The first MC sample that has been studied was the ALPGEN - Pyhtia sample where the events were generated by ALPGEN with

the CTEQ6L1 PDF and then soft parton showering, fragmentation and hadronization were done by Pythia. The b-jet production in this sample was found to disagree with the data, for this reason a second set of Z+jets background was generated.

The second and actively used Z+jets background MC sample is generated by Sherpa v1.4.1 [18] with the CT10 [19] PDF. These samples are generated in the different Z transverse momenta regions for increasing the statistics of the high-P_T events. These regions are $70-140\,\text{GeV}$, $140-280\,\text{GeV}$, $280-500\,\text{GeV}$, $500-\infty\,\text{GeV}$ and there also exists an all inclusive sample to cover the lowest P_T region. These samples combined together with truth matching applied to remove any duplications that come from the use of the all inclusive sample. The Z+jets Sherpa sample has good b-jet production and shape agreement with the data. However it needs a data driven normalization correction to obtain a good data-MC agreement. The details of this normalization are found in Section 6.4.

6.2.2. $t\bar{t}$ Background

The $t\bar{t}$ background contributes approximately 4.5% of the overall background. It is generated with Powheg r2129 [20] with CT10 (NLO) PDF and the soft parton showering, fragmentation and hadronization is done by Pythia v2.13 [21] using CTEQ6L1 (LO) [22] PDF. The $t\bar{t}$ background sample does not include the events where the $t\bar{t}$ decays all hadronically.

6.2.3. Di-Boson Background

The di-boson background is the third and the last notable background in this analysis contributing 4.5% of the overall background. It's MC sample is generated with Alpgen [23] and Herwig [24] using CTEQ6L1 (LO) PDF.

6.2.4. E_6 Signal Samples

The signal for this analysis is a pair of heavy iso-singlet quarks (each denoted as D). We assume that the E6 iso-singlet quarks that are used are the lightest iso-singlet quarks proposed in the model. The signal events are generated with CompHep v4.5.1 [25] in the process $pp \rightarrow DD \rightarrow VjVj$ (V=Z,H,W). The events that are produced by CompHep are then fed to Pythia 8 for parton showering, fragmentation and hadronization. The signal sample is generated with equal branching ration for all decay channels. For this reason, an event weight that corrects the E_6-predicted branching ratios are applied to the signal. The signal MC events has been generated with varying mass, with 100 GeV increments spanning the range of $300 - 800$ GeV. Finaly the current signal samples have a single lepton cut applied to them at the generator level. The list of list of all the samples can be found in the appendix.

6.2.5. W+Jets Background

The W+Jets background's contribution to the overall background is negligible, no W+Jets background events were able to survive the cut flow. The W+Jets backgrounds that have been used for this analysis are ALPGEN - Pythia and Sherpa samples. Both samples have been generated in the same way as the Z+jets Sherpa MC samples.

6.2.6. Single Top Background

The contribution of the single top background is minimal but it is still being used in order to improve data/MC agreement. The t-channel background sample is generated using AcerMC 3.8 [26] and hadronized through Pyhtia 8 [21]. using CTEQ6L1 PDF. The s-channel background sample is generated via MC@NLO [27] and hadronized through Herwig 2.7 [24].

6.3. Data Driven Background Samples / QCD Background

In this analysis the QCD background's contribution is expected to be minimal as the analysis makes use of a tight lepton selection and reconstructs a Z boson. In order to experimentally show that the QCD background is negligible, the FakesMacros tool is used to estimate the QCD Background. Fakes Macros tool uses the MM matrix method developed by the D0 collaboration. [28]

According to the results from the tool, in this E_6 signal search the QCD background doesn't even equate to 0.2% of the overall background. In addition, since this tool can equate negative weights to events, the QCD background also contains negative bins on different histograms. Since the QCD background is negligible and also in order to prevent negative contributions, the QCD background won't used as source of background through out this analysis. The QCD backgrounds Z P_T distribution can be found in the figures 6.1 , 6.2 for muon and electron channel.

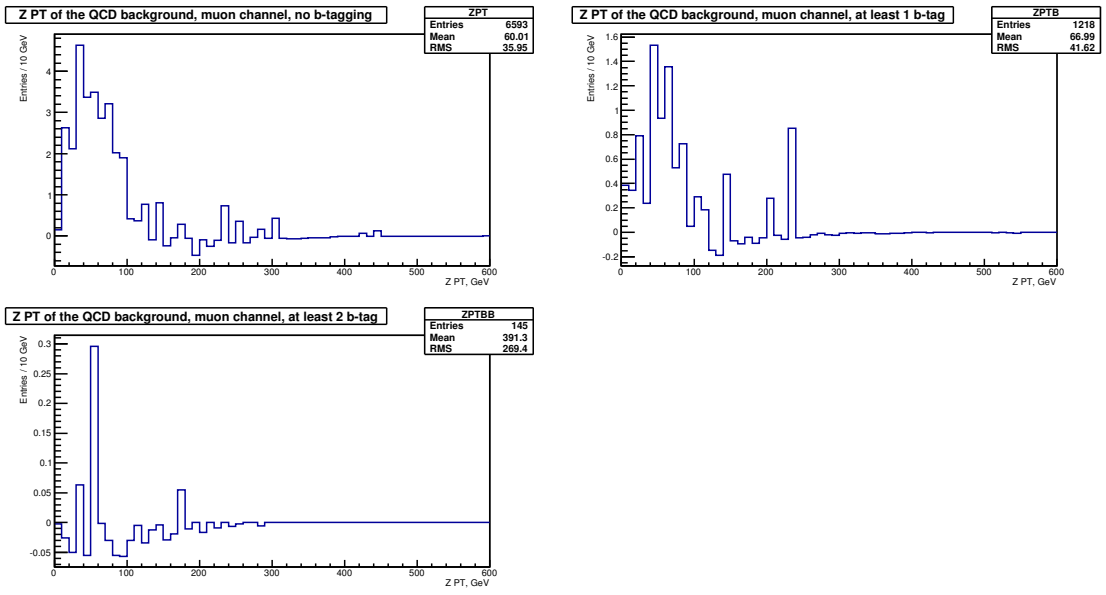

Figure 6.1. QCD Background Z P_T Distribution, Muon Channel.

6.4. Data Driven Normalization for the Z+Jets Background

As stated before, the Z+jets background composes $\approx$ 90% of the overall background. When data-MC comparison was made on kinematic variables, it was seen

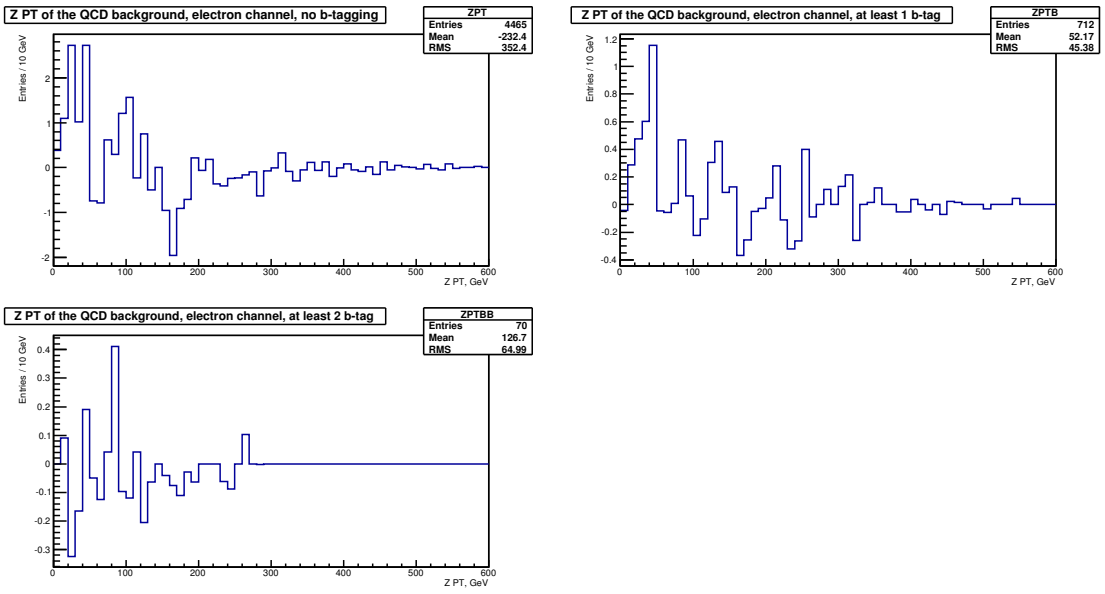

Figure 6.2. QCD Background Z P_T Distribution, Electron Channel.

that the in both electron and muon samples the total number of events in the Z+jets background sample exceeded the total number of observed data events. The distributions on figures 6.3 and 6.4 clearly identifies this problem. In order to solve this problem, a data driven renormalization is driven.

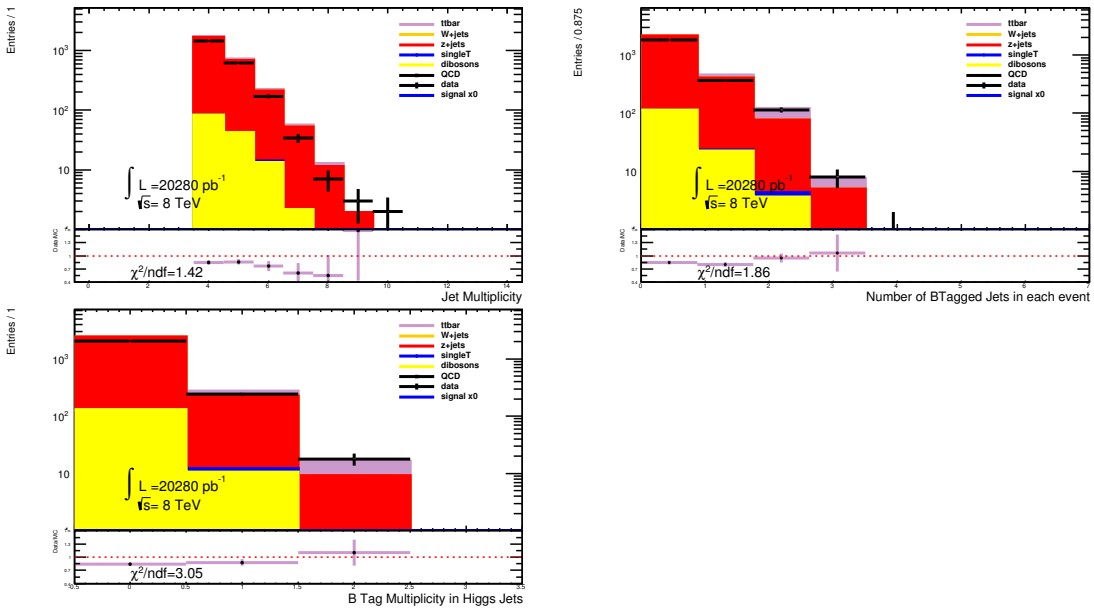

Figure 6.3. Unscaled Jet Multiplicity Histogram, Electron Channel.

To calculate the Z+jets scale factor, it is assumed that the only problematic background is the Z+jets background. Under this assumption when all backgrounds

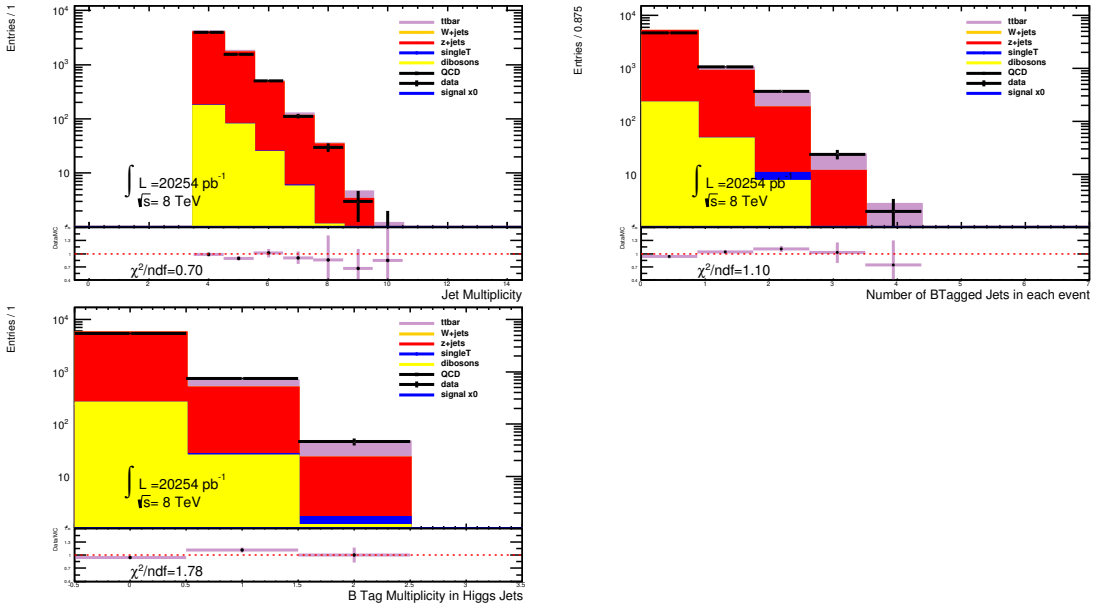

Figure 6.4. Unscaled Jet Multiplicity Histogram, Muon Channel.

except Z+jets are removed from the data, whatever is left should be Z+jets component of the data. Under this assumption when the Z+jets component of the the data is divided by the Z+jets background, the data driven scale factor is derived. If this scale factor is derived on a Data sample that could potentially carry a E_6 Signal, there is a risk of loosing potential signal events. For this reason, this data driven background is calculated over the Z veto control region. This Z veto run contains all the cuts and reconstruction algorithms of a normal run, except that the Z window is inversed to reject the events in the window and accept every other event. In addition to this there is an extra Z $P_T > 40\,\text{GeV}$ cut introduced since the Sherpa Z+jets background sample has a ZP_T cut introduced at the generator level.

The kinematics for the Z veto kinematic plots can be found in the Section 7.1. It's decided that the data driven scale factor would be calculated over the b-tag multiplicity histogram's first bin. The reason behind this is that the Higgs signal is expected to have an at least 1 b-tagged jet and from the 0-tagged bin, an extra signal veto can be done. Also 0 b-tagged bin is the Z+jets dominant bin, providing increased statistics. The figure 6.6 and 6.5 shows the b-tag multiplicity histogram and the calculated Z+jets scale factor for both channels. The top right corner of the histogram shows the calculated Z+jets normalization scale factor for that figure. For

the muon channel the scale factor is 0.934 ± 0.126 and for the electron channel it is 0.908 ± 0.231. The weighted average of them is 0.928 ± 0.111.

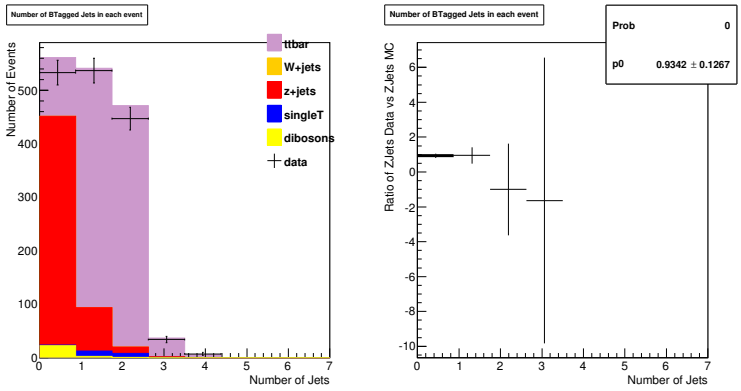

Figure 6.5. The Z Veto B-Tagged Multiplicity Histograms and Z+Jets Scale Factor, Muon Channel.

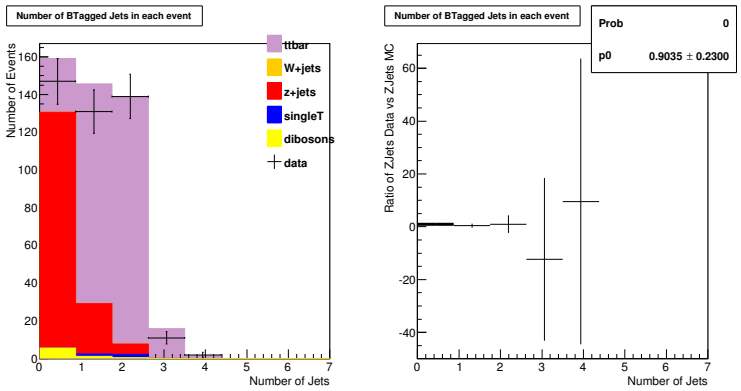

Figure 6.6. The Z Veto B-Tagged Multiplicity Histograms and Z+Jets Scale Factor, Electron Channel.

6.5. Systematic Uncertainties

The background and signal models and models of the detector are not perfect. For this reason, the MC samples have flaws. To account for these flaws, the MC samples are compared to the data in a long list of control samples by the various detector, performance groups in the ATLAS collaboration. Each of these studies yield correction factors that are used to improve the accuracy of the MC samples. However, as the determination of each of these correction factors are themselves prone to errors

Table 6.1. Background Samples And Their Total Cross Sections.

Name	**Generator**	**Total X-Section (pb)**
Z+Jets	Sherpa	3330.6
$t\bar{t}$	Powheg+Pythia	114.51
Di-Boson	Alphen+Herwig	43.1
Single-Top t-channel	AcerMC+Pythia	25.8
Single-Top s-channel	MC@NLO+Herwig	21.7
W+Jets	Sherpa	34088

(mainly because of the statistics of the control samples), these errors need to be propagated to the final result of the analysis.

In order to accomplish this, we rerun the whole analysis chain multiple times, changing each correction factor up and down by its own uncertainty (i.e $\pm\sigma$). Finally when we are setting the limits, we feed all the modified histograms into the limit setter, taking into account which systematic effects are correlated and which are independent.

In this analysis the following uncertainties have been taken into account: jet energy smearing, jet energy scaling, muon scale factor, muon P_T smearing, muon trigger efficiency, electron energy scaling, electron scale factors, background uncertainties, Z+jets data-driven scale factor. The overall list of uncertainties and their contributions can be found in Tables 6.2 and 6.3.

6.5.1. Jet Uncertainties

In ATLAS the jet reconstruction is a complicated process and with the fragmented nature of the jets, the jets' energies are mis-calculated. In-order to correct these errors, energy correction is done. To account for these corrections the jet energy resolution systematics are applied. In addition to this, sometimes real jets can be lost during the object reconstruction phase, to calculate the effects of the jet losses, jet energy reconstruction uncertainty is applied.

To account of the non-linear reconstruction effects of the ATLAS detector, the (JES) uncertainties have been driven. There are three kinds of JES uncertainties, they are close-by jets systematics, flavor composition systematic and the flavor response systematic. These systematics depends on the jets' isolation, P_T and η. The flavor composition systematic calculates the error bars on how many light quarks and gluons exists in the analysis. Lastly the flavor response systematic measures the flavor response for the light quarks and gluons by exploiting the topology of the jets. The Last Jet Uncertainty is the b-tag scale factor, this scale factor is already used in the analysis but because of technical difficulties they are not available.

6.5.2. Muon Uncertainties

Different scale factors are applied to MC muon objects inorder to correct their generator level errors, which are the trigger scale factor and muon reconstruction efficiency. These scale factors holds their own uncertainties that should be noted in the calculation of the percentage of error. Also as muon objects are reconstructed, potential errors can occur such as faulty reconstruction of muon energy. To correct this mistake muon energies are smeared $\pm\sigma$ inoder to estimate the error bars of the muon energy reconstruction.

6.5.3. Electron Uncertainties

The electron reconstruction suffers from similar problems. For this reason the electron objects also have scale factors applied. These scale factors are reconstruction scale factor, trigger scale factor and identification scale factor. As it is with all scale factors, they come with their own error bars.

To account for electron energy looses, the electron it self is smeared by default. This energy smearing also comes with its error bars. To account for the effect of this smearing, the uncertainty of these effects are calculated.

6.5.4. Background Uncertainties

The MC background samples also hold uncertainties caused by its theoretical uncertainties. (The uncertainty effects each MC sample separately and they depend on PDF selections and MSTW prescriptions.) To estimate these uncertainties, the same MC samples are run by different PDF selections and MSTW prescriptions. From their differences in their cros-sections an uncertainty is derived.

In addition to these uncertainties the Z+jets sample have an uncertainty caused by the Z+jets scale factor that was driven.

6.5.5. Luminosity Uncertainty

Currently for the $20fb^{-1}$ the uncertainty is $\pm 2.6\%$.

Table 6.2. Uncertainties, Muon (Taken form M_{D_Z} Distribution).

Uncertainty	**Z+jets** (%)	$t\bar{t}$ (%)	**Di-Boson** (%)	**Single-Top** (%)	E_6 **Signal** (%)
Luminosity Uncertainty	+2.6 / -2.6	+2.6 / -2.6	+2.6 / -2.6	+2.6 / -2.6	+2.6 / -2.6
Cross-Section Uncert	+11.1/-11.1	+11/-11	+34/-34	+7/-7	+0/-0
μ Reconstruction	+0.76/-0.076	+0.72/-0.71	+0.76/-0.75	+0.75 /-0.74	+0.0/+1.5
μ Smear	+0.006/0	+0.12/-0.3	+8.4/-0.0	+0.35/0	+1.07/-0.77
μ Identification	+0.006/-0.012	+0.0/-0.51	0.0 / 0.0	+0.18/0	+0.77/-0.77
μ P_T Scale	+0.012/-0.00063	+0.6/-0.1	8.4/-0.0	+0.16/0	+0.77/-0.77
μ Trigger Scale	+1.98/-0.64	+2.24/-1.1	1.9/-0.64	+2.29/-1.15	+1.35/-0.01
Jet Scale	+6.66/-0.05	+4.70/-3.5	+0/-0	+7.29/-3.69	+1.5/-1.5
Jet Reconstruction	+0.027/-0.027	+0.0/-0.0	+0.0/0.0	+0/+0	+0.77/-0.77
Jet Energy Reco.	+0.36/-0.36	+0.65/-0.65	+7.3 / -7.3	+2.28/-2.28	+6.62/-6.62
Z+Jets data driven correction	+11/-11	+0/-0	+0/-0	+0/-0	+0/-0

Table 6.3. Uncertainties, Electron (Taken form M_{D_Z} Distribution).

Uncertainty	**Z+jets** (%)	$t\bar{t}$ (%)	**Di-Boson** (%)	**Single-Top** (%)	E_6 **Signal** (%)
Luminosity Uncertainty	+2.6 / -2.6	+2.6 / -2.6	+2.6 / -2.6	+2.6 / -2.6	+2.6 / -2.6
Cross-Section Uncert	+11.1/-11.1	+11/-11	+34/-34	+7/-7	+0/-0
Ele. Reco. Scale	+0.62/-0.62	+0.49/-0.49	+0.64/-0.64	+0.66 /-0.65	+0.0/+1.5
Ele. Identification	+1.6/-1.6	+1.4/-1.5	+2.0/-1.9	+1.7/-1.7	+1.1/-2.7
Ele. Trigger Scale	+0.77/-0.77	+0.43/-0.51	+0.79 /-0.79	+0.69/-0.68	+8.27/-1.79
Ele. Energy Rescale	+0/-0.12	+0/-0.93	0/-0.35	+0.0/0.7	+0.78/-0.16
Jet Scale	+6.66/-7.87	+8.66/-5.32	+0/-0	+6.3/-12.64	+4.0/-4.0
Jet Reconstruction	+0.02/-0.02	+0/-0	+0.0/0.0	+0/+0	+0.78/-0.78
Z+Jets data driven correction	+11/-11	+0/-0	+0/-0	+0/-0	+0/-0

7. RESULTS

7.1. The Control Region

In order to validate the background MC samples, a control run has been made. The properties of this control run is that the control run is exactly the same with the E_6 analysis with the difference of having the Z window cut reversed in order to make it into a Z veto cut and adding an addition $M_Z > 40\,\text{GeV}$ cut to remove the regions where the Z is not modeled (due to a generator-level cut in Sherpa). This provides a data sample where a leptonic E_6 signal is suppressed. In this sample the dominant background is no longer the Z+jets background but it still has a significant contribution. The dominant background is from $t\bar{t}$ events. The $t\bar{t}$ contribution becomes extremely important in the b-tagged analysis since the Z+jets background has a minimal contribution to the b-tagged events.

This control region has 11 different distributions to validate the Data / MC agreement. In addition, these distributions are studied thrice for three different b-tagging choices. Lastly considering the two flavors of leptons, the total number of studied histograms plots becomes 66. These include jet multiplicity; b-tag multiplicity ; b-tag multiplicity of Higgs jets; η and ϕ distributions of leptons and jets and lastly P_T distributions of leptons, jets, leading jets and the reconstructed Z boson. Among all these comparisons, worst χ^2/ndf is 0.76, so with such good agreement, in this chapter we only show some representative distributions.In the distributions where two b-tags are required, essentially the $t\bar{t}$ background is being tested. Also, as the $t\bar{t}$ sample is validated, the Z+jets data-driven scale factor becomes more reliable. Also in these plots the Z+jets data-driven scale factors have been used, which provides a validation for the whole procedure.

Starting with the most important distributions, on plots 7.1 and 7.3 lies the histograms of the jet multiplicity, b-tag multiplicity and the b-tag multiplicity of Higgs

jets for the muon Channel. According to these plots there is near perfect agreement in jet multiplicity distributions. As the b-tagging options tightens the statistics goes lower but all plots still lies within the error bars. The electron channel equivalent of the same kinematic plots are 7.2 and 7.3. These distributions have a worse reconstruction efficiency compared to the muon channel for this reason the statistics are lower then the muon channel. With lower statistics the MC data agreement of the electron channel is worse then the muon channel but the histograms still show a good agreement of data with the MC.

The plot 7.4 , 7.5, 7.6 and 7.7 shows the lepton and jet η, ϕ distributions . According to these plots for the 0 tagged case, the η, ϕ distributions have good agreement with slight statistical disturbances. For the exactly two b-tagged analysis, the statistics are too low to form an uniform distribution but everything is within the error bars. The last set of distributions, plots the P_T distribution of the leptons, jets and the reconstructed Z boson in order to prove that the particles have been modeled correctly. According to the plots 7.8 , 7.9, 7.10 and 7.11 the P_T distributions for both muon and electron channels have nice data-MC agreement, even when the statistics are small.

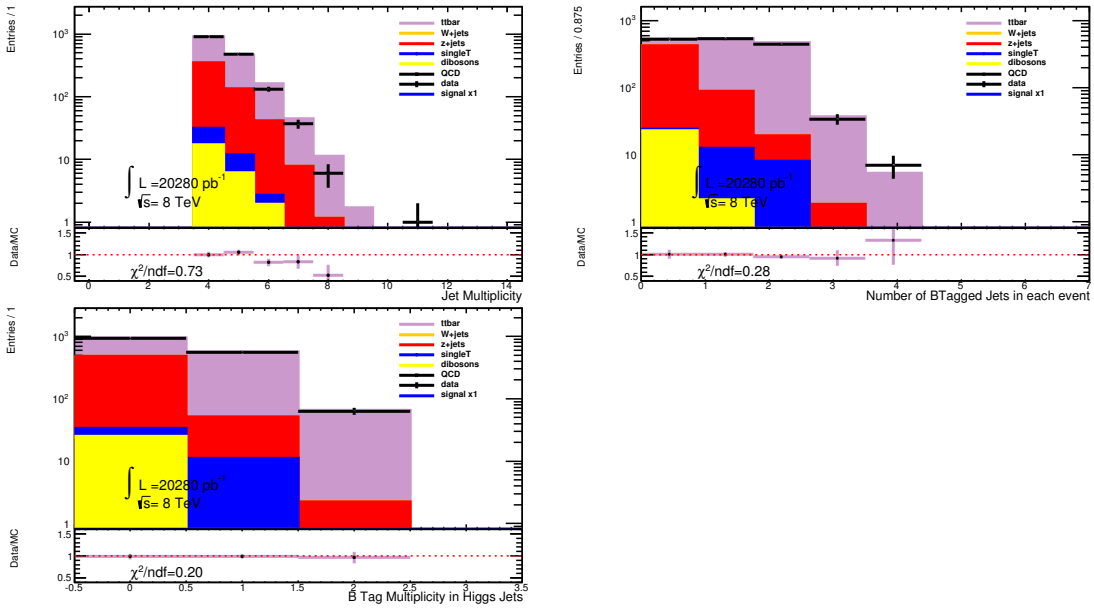

Figure 7.1. Multiplicity Histograms For The Z Veto Control Region, No B-Tagging Forced, Muon Channel.

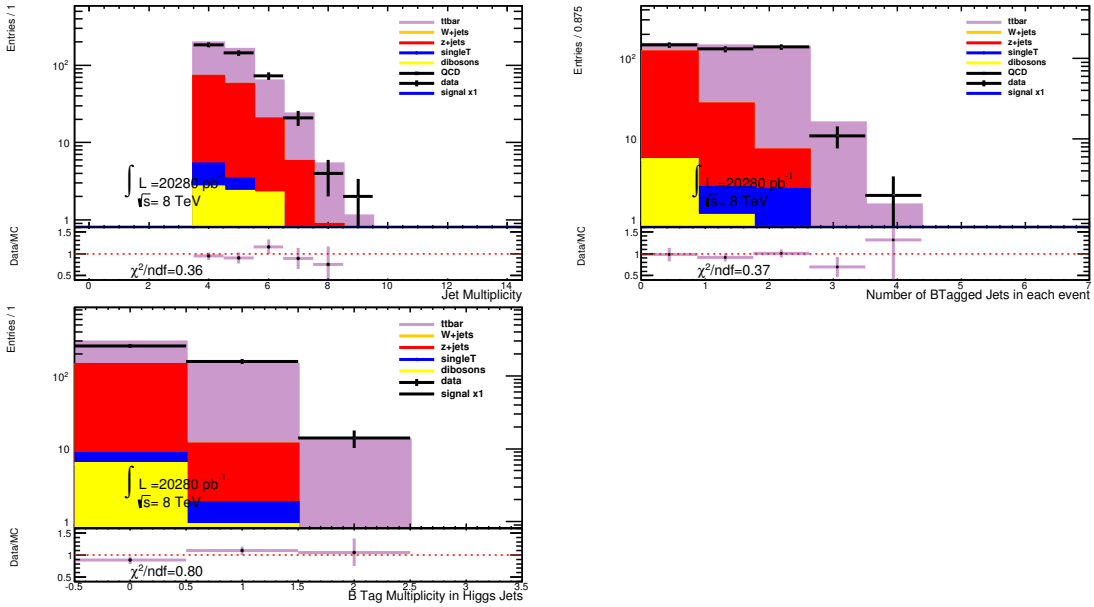

Figure 7.2. Multiplicity Histograms For The Z Veto Control Region, No B-Tagging Forced, Electron Channel.

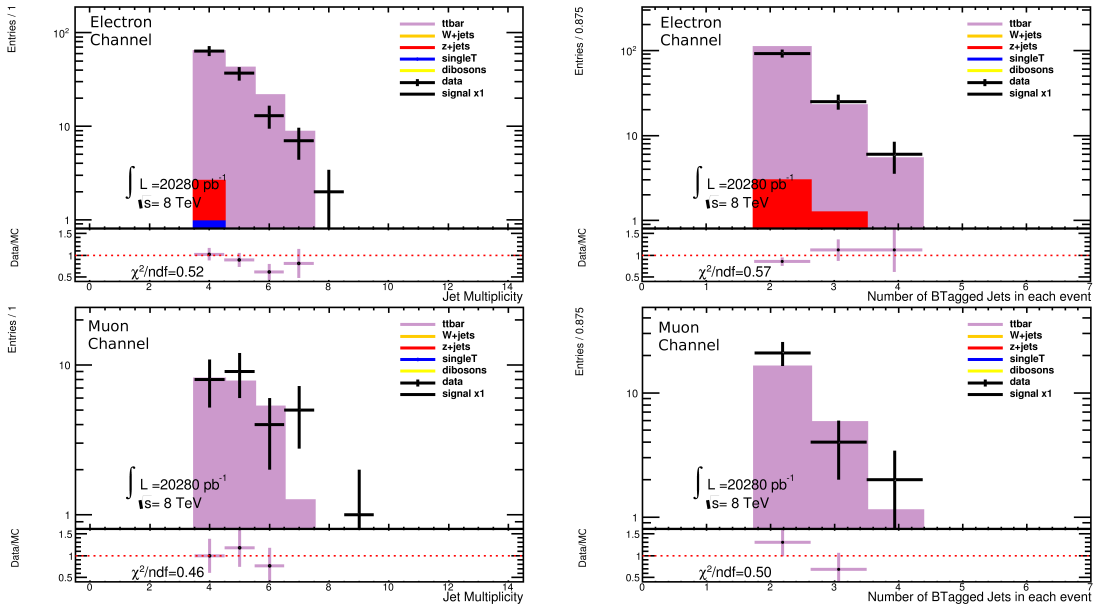

Figure 7.3. Multiplicity Histograms For The Z Veto Control Region, Two B-Tagged Jets Are Required, Muon Channel And Electron Channel.

7.2. Analysis Results

After background validation, the analysis is ready to be unblinded. For limit setting purposes, at least one of the jets that forms a Higgs boson are required to

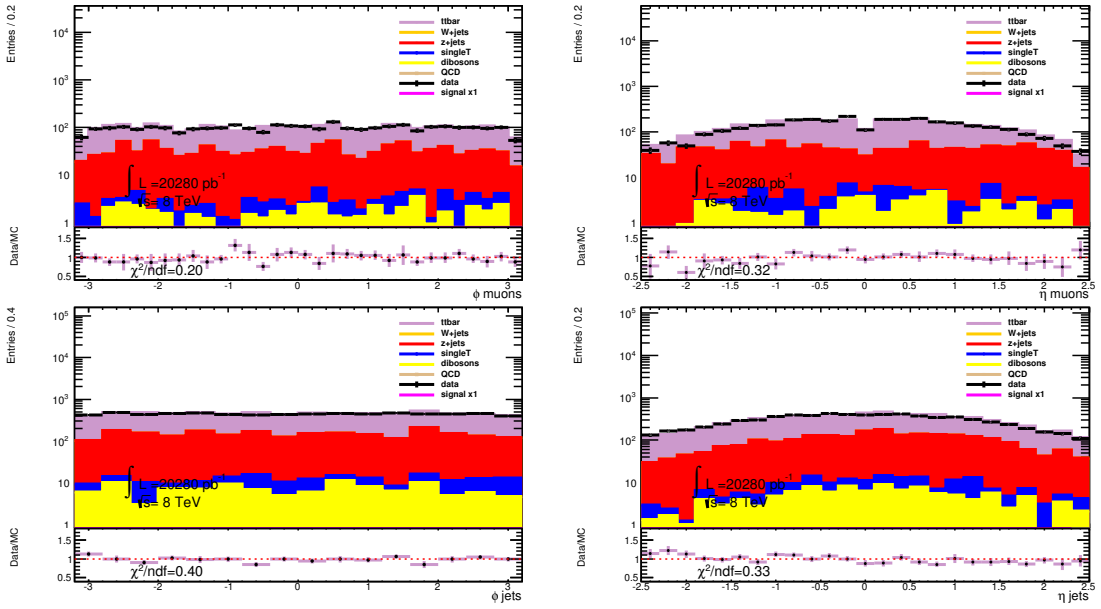

Figure 7.4. η And ϕ Distribution For The Muons And Jets, No B-Tagging Forced, Muon Channel.

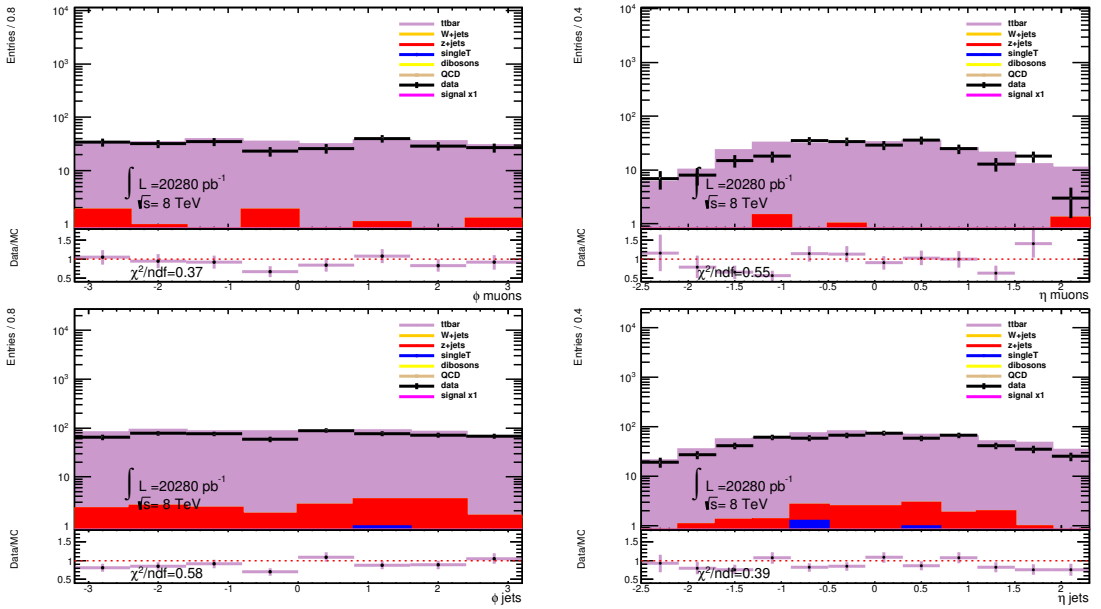

Figure 7.5. η And ϕ Distribution For The Muons And Jets, Two B-tagged Jets Are Required, Muon Channel.

b-tagged while the double b-tagged forced sample has low statistics and 0 b-tagged sample includes feed through from other backgrounds samples.

The figure 7.12 and 7.13 shows the unblinded P_T distributions for the leptons / jets and the mass distribution for the Z / Higgs bosons with a signal mass at 500 GeV,

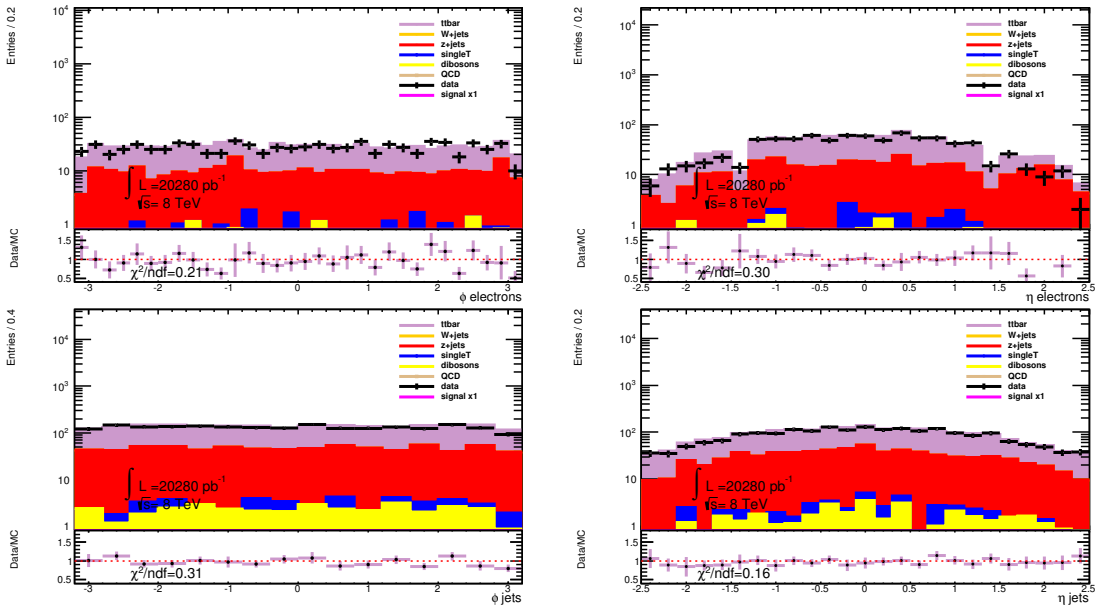

Figure 7.6. η And ϕ Distribution For The Muons And Jets, No B-Tagging Forced, Electron Channel.

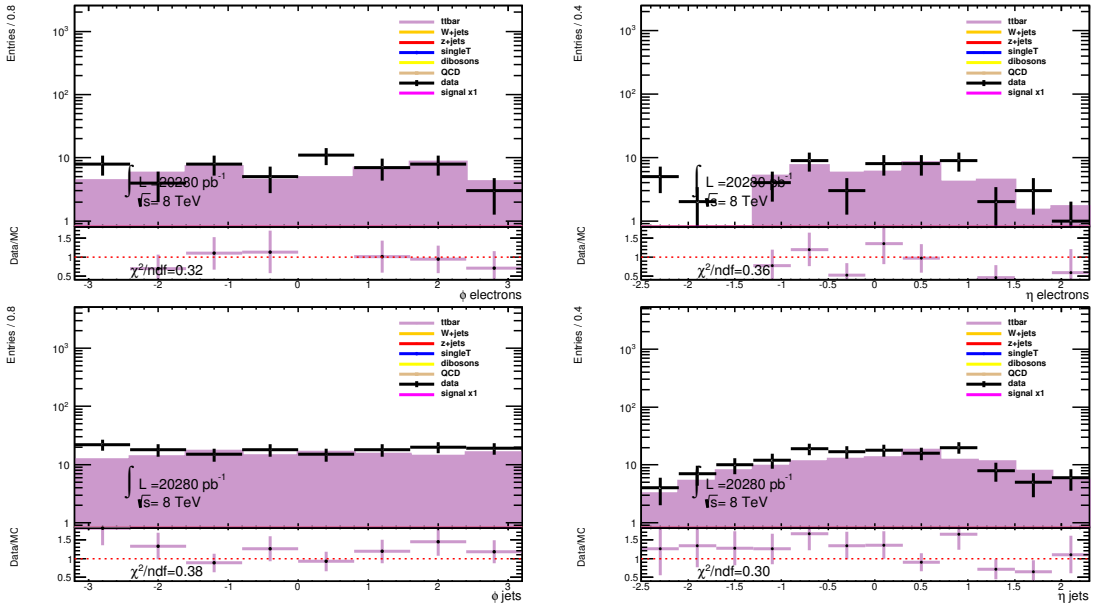

Figure 7.7. η And ϕ Distribution For The Muons And Jets, Two B-tagged Jets Are Required, Electron Channel.

providing a control basis for the H_T and M_{D_Z} unblinded plots. According to these two distributions the current MC samples have a good agreement with data.

On figures 7.14 and 7.15 lies the discriminant H_T plot with a signal mass at 500 GeV. According to these plots no excess events has been observed in the signal

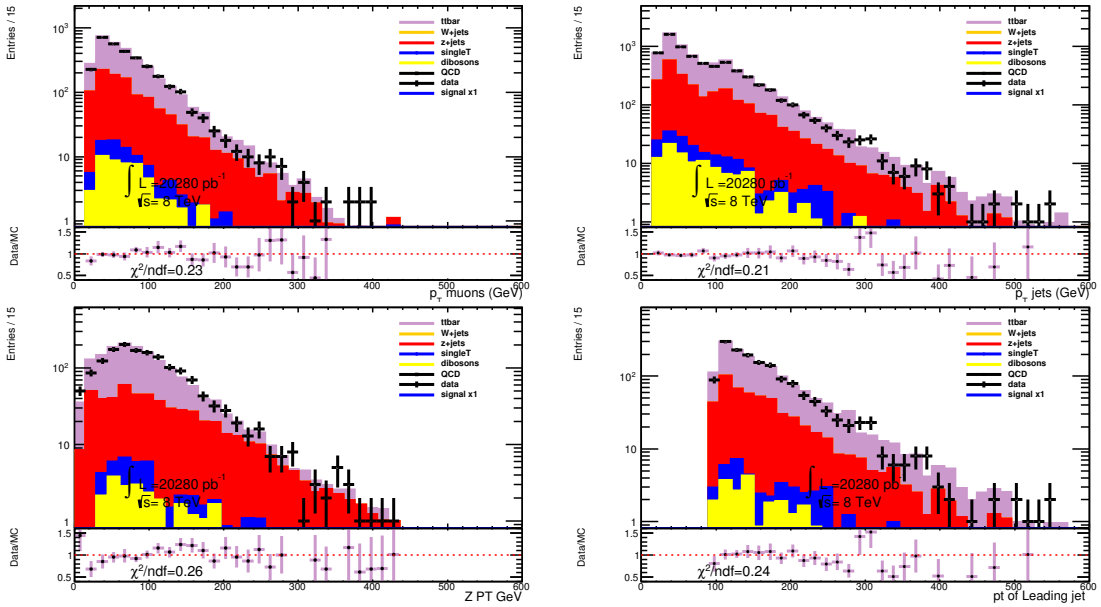

Figure 7.8. P_T Distributions For The Muons, Jets And Reconstructed Objects; No B-Tagging Forced; Muon Channel.

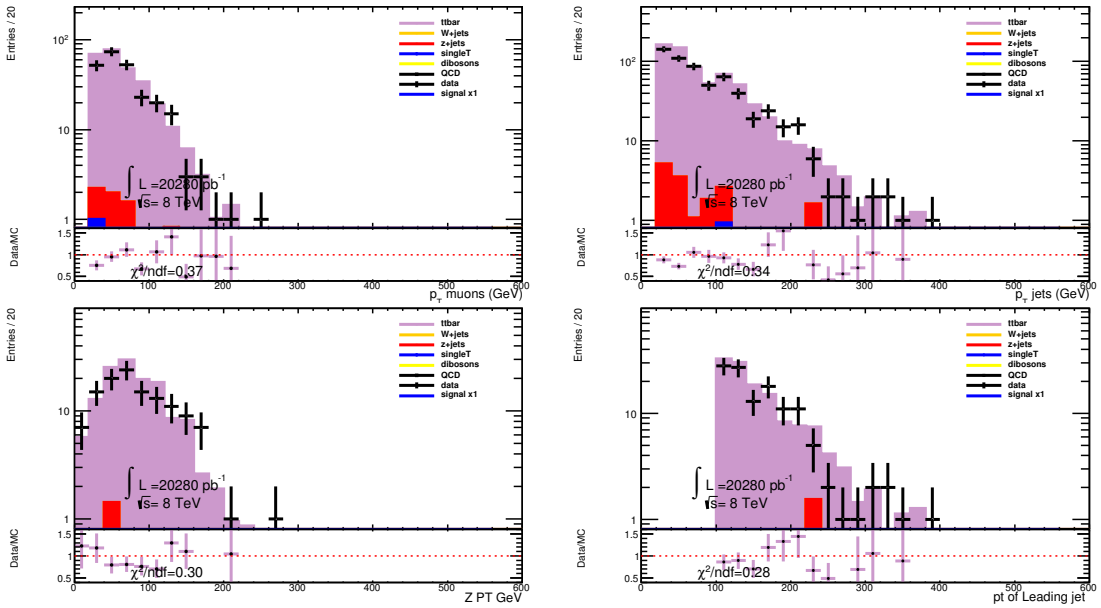

Figure 7.9. P_T Distributions For The Muons, Jets And Reconstructed Objects; Two B-tagged Jets Are Required; Muon Channel.

region. The signal region has a good agreement with the SM.

On figures 7.16 and 7.17 is the discriminant M_{D_Z} plot with a signal mass at 500 GeV. No signal like excess events has been observed in M_{D_Z} distributions, every-

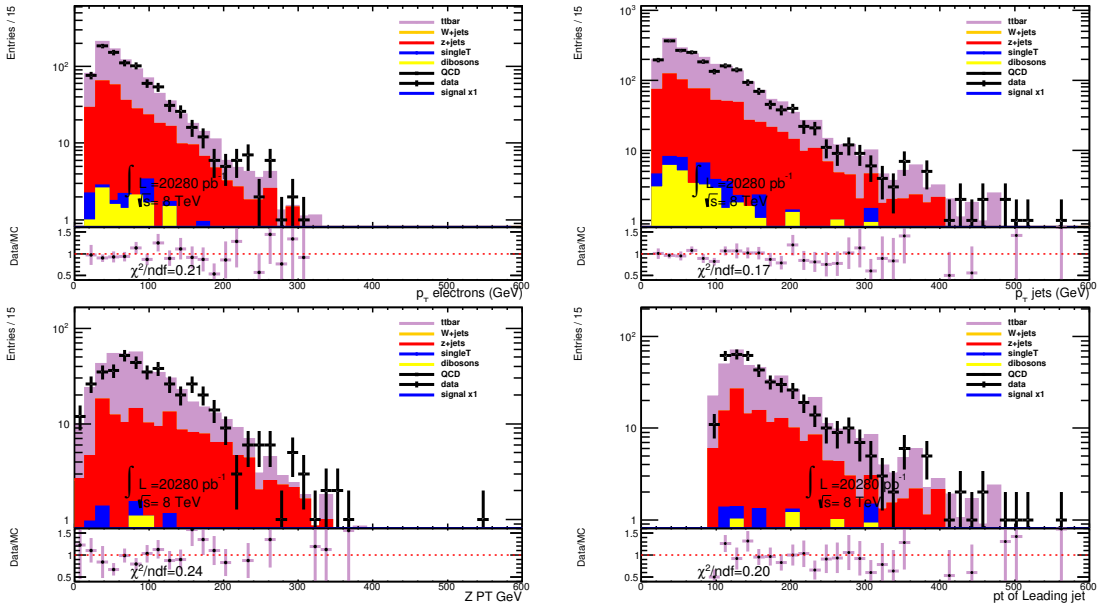

Figure 7.10. P_T Distributions For The Electrons, Jets And Reconstructed Objects; No B-Tagging Forced; Electron Channel.

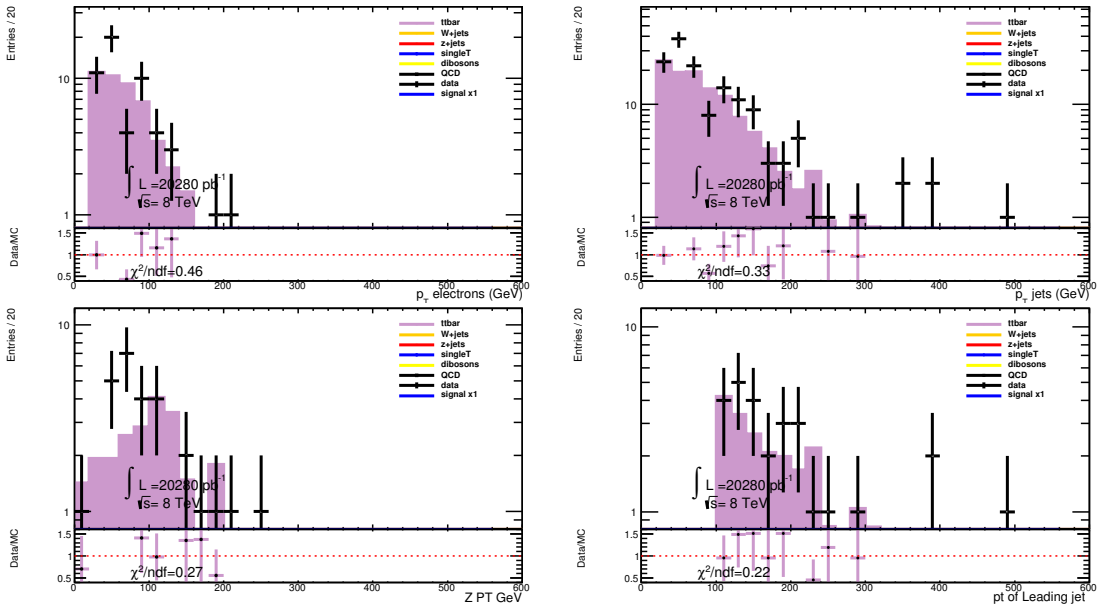

Figure 7.11. P_T Distributions For The Electrons, Jets And Reconstructed Objects; Two B-Tagged Jets Are Required; Electron Channel.

thing is within limits of the theoretical expectations of the SM theory.

As no signal events have been observed, 95% upper limit can be set for the pair produced iso-singlet quark at the proton proton collusions in the LHC. The figure 7.18

shows the 95% CL cross-section limits, showing the newly proposed limit at 490 GeV.

Instead of searching for an E_6 iso-singlet quark, the analysis can also search for heay quarks that decays only via the flavor changing neutral quarks. The figure 7.19 shows the 95% CL cross-section limit for this heavy quark. According to this plot shows that this heavy quark can be excluded upto a limit at 730 GeV.

The MCLimit tool [29] has been used for limit setting. The tool uses the CL_S method [30] [31]. Which is a log-likelihood method to examine the data under the background and signal+background hypothesis to put a limit on the proposed quarks.

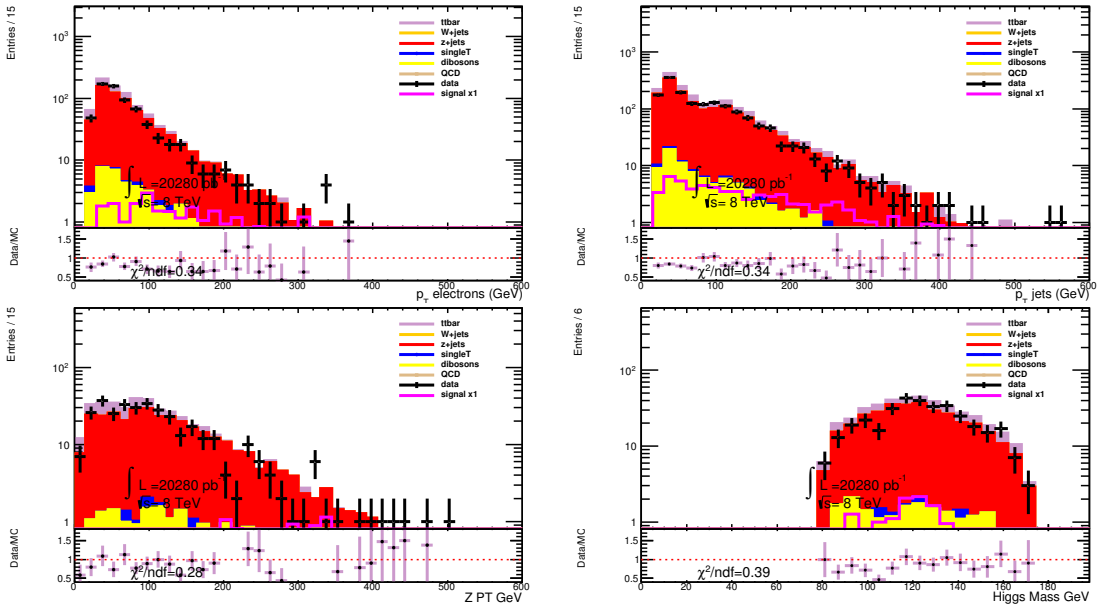

Figure 7.12. P_T Distributions For The Electrons, Jets And Reconstructed Objects; 1 B-Tag Required; Electron Channel; Signal Region.

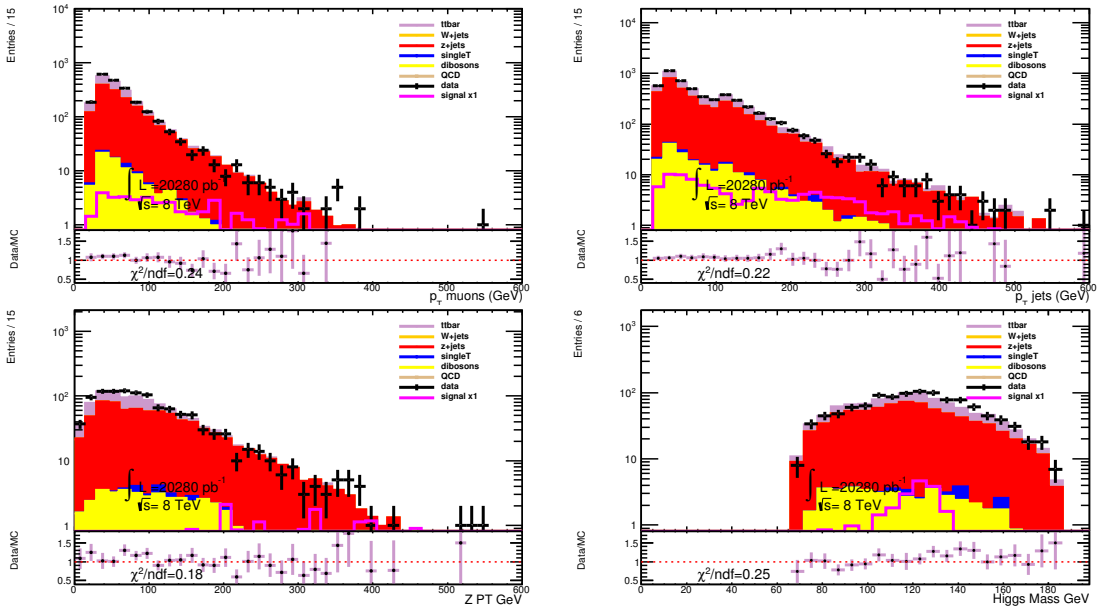

Figure 7.13. P_T Distributions For The Muons, Jets And Reconstructed Objects; 1 B-Tag Required; Muon Channel; Signal Region.

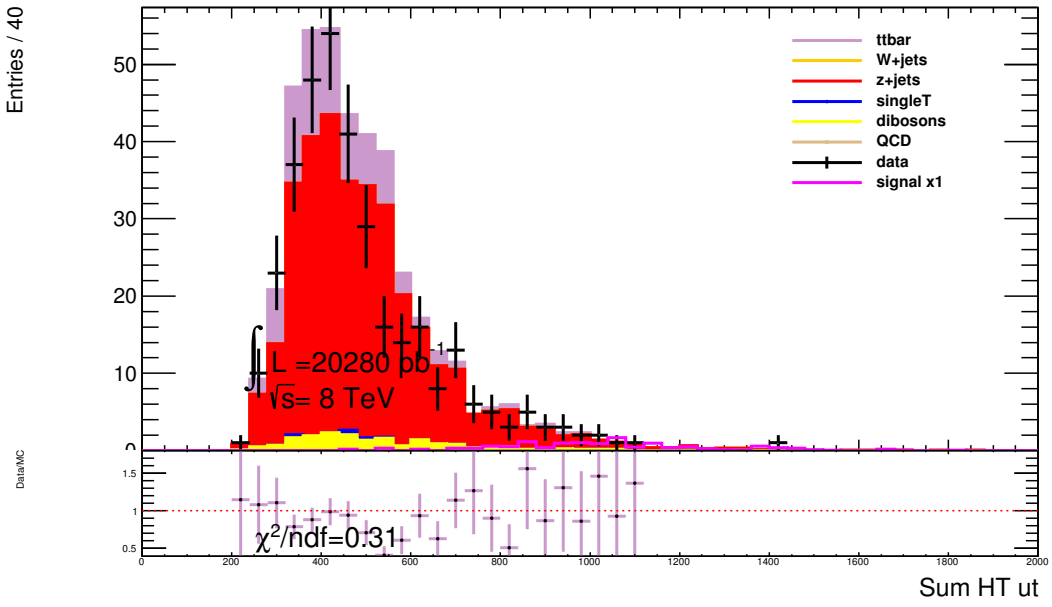

Figure 7.14. H_T Distribution, 1 B-Tag Required, Electron Channel, Signal Region.

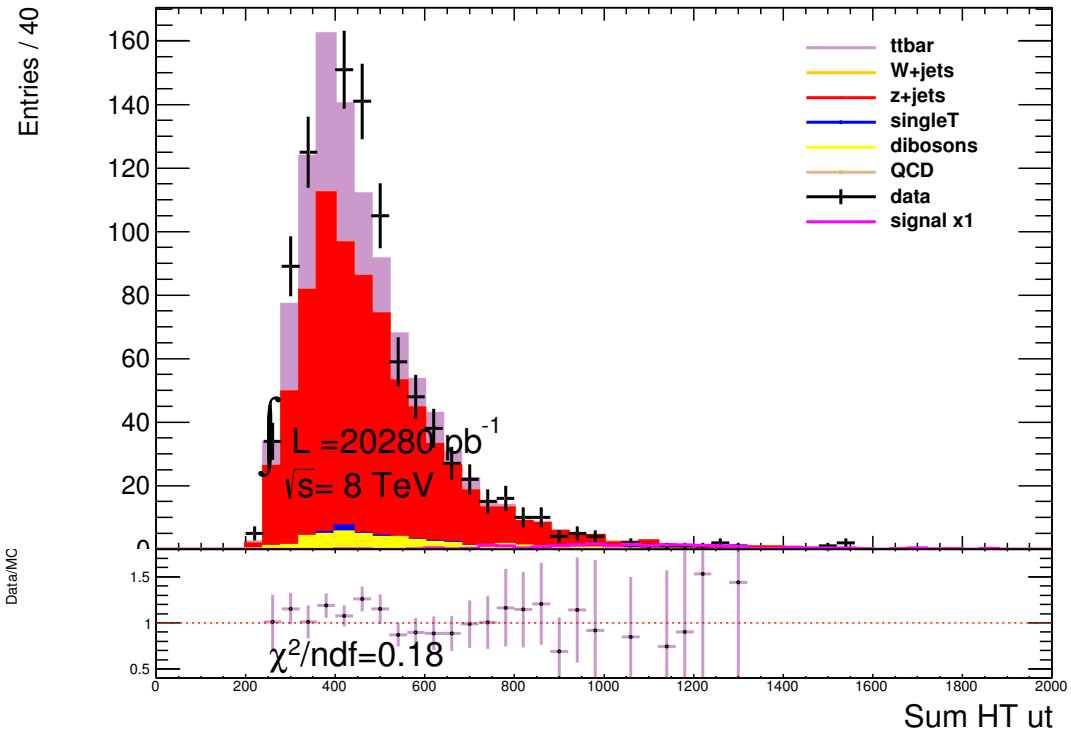

Figure 7.15. H_T Distribution, 1 B-Tag Required, Muon Channel, Signal Region.

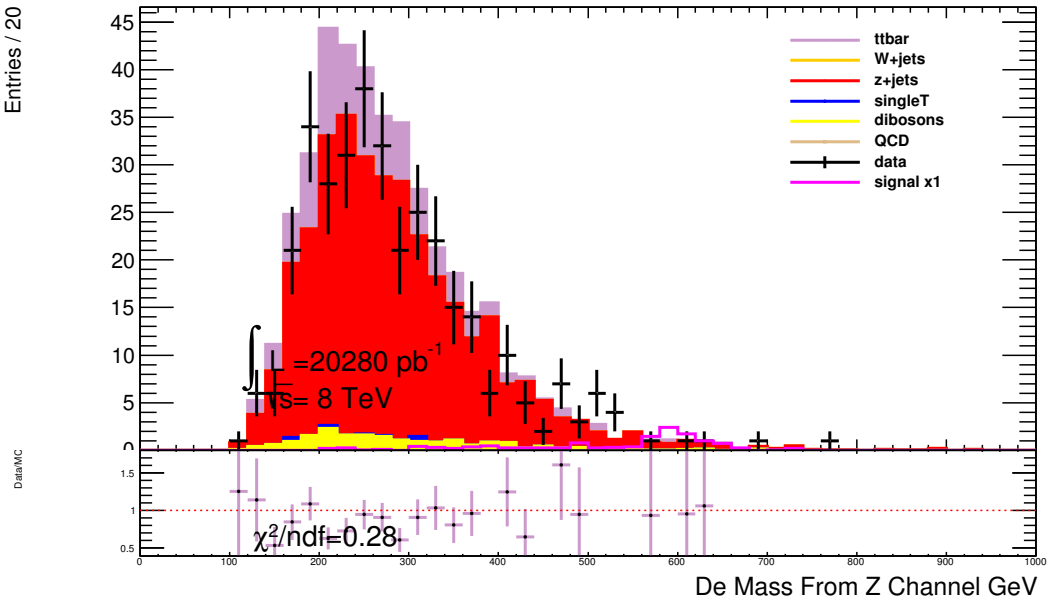

Figure 7.16. Discriminant M_{D_Z} Distribution, 1 B-Tag Required, Electron Channel, Signal Region.

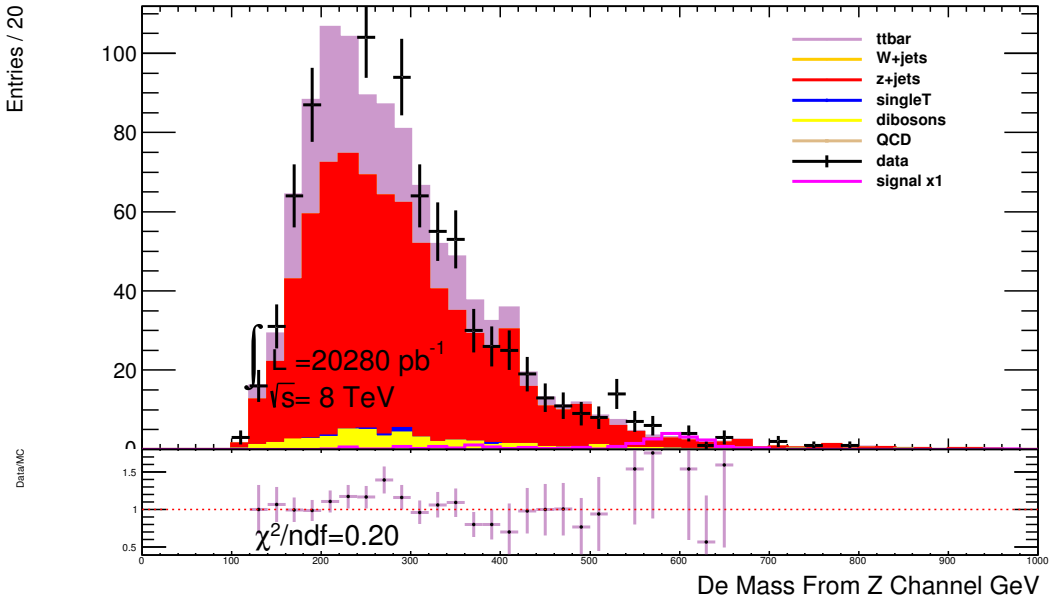

Figure 7.17. Discriminant M_{D_Z} Distribution, Jets And Reconstructed Objects; 1 B-Tag Required; Muon Channel; Signal Region.

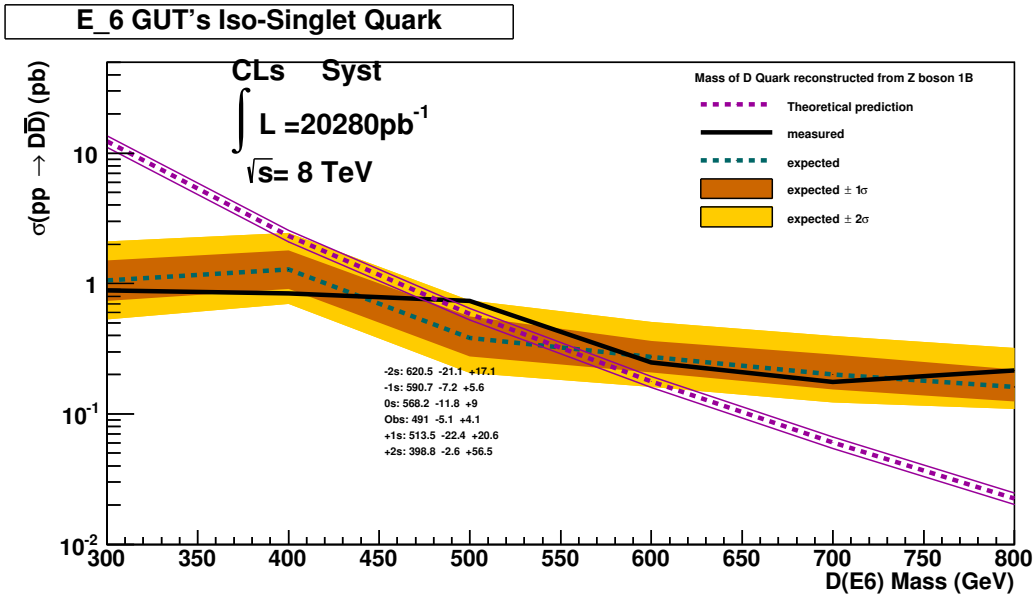

Figure 7.18. The Combined Limit With 95% CL, M_{D_Z} Distribution Is Used As The Discriminant.

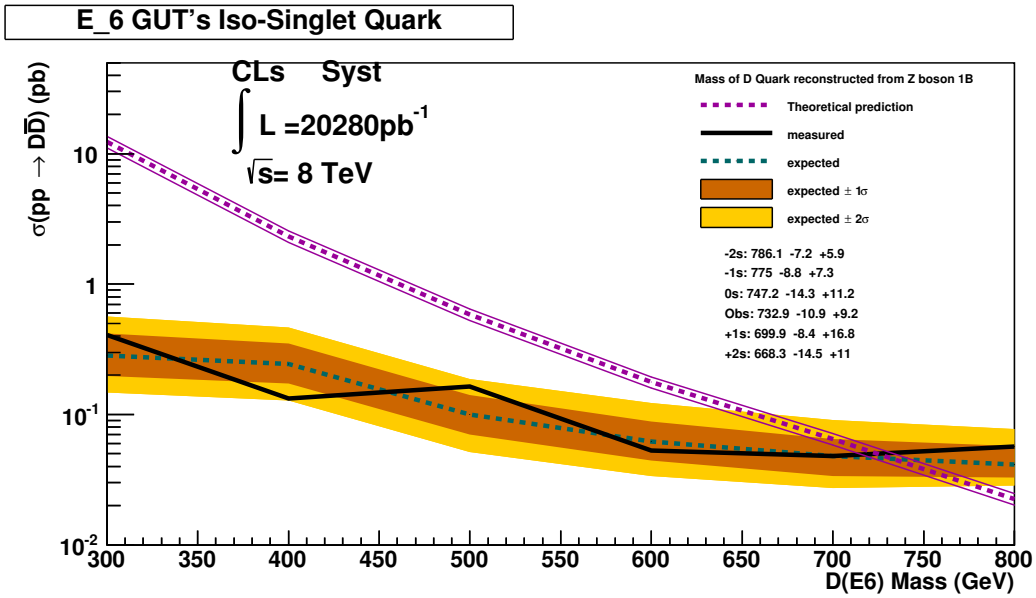

Figure 7.19. The Combined Limit With 95% CL For A Quark Decaying only Via Flavor Changing Neutral Current, M_{D_Z} Distribution Is Used As The Discriminant.

8. CONCLUSION

In this thesis the E_6 iso-singlet quark pair production at LHC has been analyzed. The iso-singlet quark analysed in this analysis belongs to the up-down quark family, which is theoretically expected to be lightest of the E_6 iso-singlet quarks. Keeping this in mind, no family specific cut has been aplied in this analysis, keeping the analysis sensitive to all the families of the iso-singlet quarks . The search for iso-singlet quark has been done over the data set recorded by the ATLAS detector which corresponds to $20\,\mathrm{fb}^{-1}$ total integrated luminosity collected from proton proton collisions at c.om. energy of 8 TeV provided by the LHC at CERN.

A specific decay channel of the E_6 iso-singlet quark has been analyzed. The analysis examines the events where the quark pair decays via $pp \rightarrow DD \rightarrow HjZj \rightarrow 4j\,2l$ channel. The events that are reconstructed are expected to have four jets (at least on should be b tagged) and a Z boson candidate that has been reconstructed from two leptons. A χ^2 algorithm is used in the reconstruction of the events. Under these prescriptions, no excess events have been observed under the Standard Model expectations. According to the iso-singlet quark decay branching ratios foreseen by the E_6 GUT theory, quarks masses below 490 GeV has been excluded at the 95% confidence level, while the expected limit based on MC studies is 560 GeV. Also for a quark that decays only via the flavor changing neutral current, the mass lower then 730 GeV is excluded with the 95% confidence level.

The analysis that requires the events to contain 2 b-tagged jets has also been analyzed. This b-tagging option provides a very good signal to background ratio, However due to the lack of statistic this option has not been used.

REFERENCES

1. Istin, S., "Search For E_6 Quarks In Z Channel", *To Be Published*.

2. Hedberg, V., "Images Of Various Parts Of The Atlas Detector", `http://hedberg.web.cern.ch/hedberg/home/atlas/atlas.html`, 2009, [Accessed June 2014].

3. Beringer, J. *et al.*, "Review of Particle Physics", *Physical Review Letters D*, Vol. 86, p. 010001, 2012.

4. *Constraints On The Higgs Boson Width From Off-Shell Production And Decay To ZZ To llll And llvv*, Tech. Rep. CMS-PAS-HIG-14-002, CERN, Geneva, 2014.

5. Georgi, H. and S. Glashow, "Unity Of All Elementary-Particle Forces", *Physical Review Letters*, Vol. 32, No. 8, pp. 438–441, 1974.

6. Gürsey, F., P. Ramond and P. Sikivie, "A Universal Gauge Theory Model Based on E_6", *Physics Letters*, Vol. 60B, No. 2, pp. 177–180, 1976.

7. Mehdiyev, R., S. Sultansoy, G. Unel and M. Yilmaz, "Prospects To Search For E_6 Isosinglet Quarks In ATLAS", *The European Physics Journal C*, Vol. 49, pp. 613–622, 2007.

8. Sultansoy, S. and G. Unel, "The E_6 Inspired Isosinglet Quark And The Higgs Boson", *Physics Letters B*, Vol. 669, No. 1, pp. 39 – 45, 2008.

9. Bajc, B. and V. Susič, "Towards The Minimal Renormalizable Supersymmetric E_6 Model", *Journal Of High Energy Physics*, Vol. 1402, p. 058, 2014.

10. Aliev, M., H. Lacker, U. Langenfeld, S. Moch, P. Uwer *et al.*, "HATHOR: Hadronic Top and Heavy Quarks Cross Section Calculator", *Computer Physics*

Communications, Vol. 182, pp. 1034–1046, 2011.

11. Lamont, M., "Status Of The LHC", *Journal of Physics: Conference Series*, Vol. 455, No. 1, p. 012001, 2013.

12. *Performance Of The ATLAS Inner Detector Track And Vertex Reconstruction In The High Pile-Up LHC Environment*, Tech. Rep. ATLAS-CONF-2012-042, CERN, Geneva, 2012.

13. "Electron Performance Measurements With The ATLAS Detector Using The 2010 LHC Proton-Proton Collision Data", *European Physics Journal C*, Vol. 72, No. arXiv:1110.3174. CERN-PH-EP-2011-117, p. 1909. 45 p, 2011, comments: 33 pages plus author list (45 pages total), 24 figures, 12 tables, submitted to Eur. Phys. J. C.

14. *Expected Electron Performance In The ATLAS Experiment*, Tech. Rep. ATL-PHYS-PUB-2011-006, CERN, Geneva, 2011.

15. *Preliminary Results On The Muon Reconstruction Efficiency, Momentum Resolution, And Momentum Scale In ATLAS 2012 pp Collision Data*, Tech. Rep. ATLAS-CONF-2013-088, CERN, Geneva, 2013.

16. *Jet Energy Measurement And Systematic Uncertainties Using Tracks For Jets And For B-Quark Jets Produced In Proton-Proton Collisions At* $\sqrt{s} = 7$ *TeV In The ATLAS Detector*, Tech. Rep. ATLAS-CONF-2013-002, ATLAS-COM-CONF-2012-070, 2013.

17. Cacciari, M., G. P. Salam and G. Soyez, "The Anti-k_t Jet Clustering Algorithm", *Journal of High Energy Physics*, Vol. 04, No. arXiv:0802.1189. LPTHE-07-03, p. 063. 12 p, 2008.

18. Gleisberg, T., S. Hoeche, F. Krauss, M. Schonherr, S. Schumann *et al.*, "Event Generation With SHERPA 1.1", *Journal Of High Energy Physics*, Vol. 0902, p.

007, 2009.

19. Lai, H.-L., M. Guzzi, J. Huston, Z. Li, P. M. Nadolsky *et al.*, "New Parton distributions For Collider Physics", *Physical Review Letters*, Vol. D82, p. 074024, 2010.

20. Frixione, S., P. Nason and C. Oleari, "Matching NLO QCD Computations With Parton Shower Simulations: The POWHEG Msethod", *Journal Of High Energy Physics*, Vol. 0711, p. 070, 2007.

21. Sjostrand, T., S. Mrenna and P. Z. Skands, "PYTHIA 6.4 Physics And Manual", *Journal Of High Energy Physics*, Vol. 0605, p. 026, 2006.

22. Pumplin, J., D. Stump, J. Huston, H. Lai, P. M. Nadolsky *et al.*, "New Generation Of Parton Distributions With Uncertainties From Global QCD Analysis", *Journal Of High Energy Physics*, Vol. 0207, p. 012, 2002.

23. Mangano, M. L., M. Moretti, F. Piccinini, R. Pittau and A. D. Polosa, "ALPGEN, A Generator For Hard Multiparton Processes In Hadronic Collisions", *Journal Of High Energy Physics*, Vol. 0307, p. 001, 2003.

24. Corcella, G., I. Knowles, G. Marchesini, S. Moretti, K. Odagiri *et al.*, "HERWIG 6: An Event Generator For Hadron Emission Reactions With Interfering Gluons (Including Supersymmetric Processes)", *Journal Of High Energy Physics*, Vol. 0101, p. 010, 2001.

25. Boos, E., V. Bunichev, M. Dubinin, L. Dudko, V. Edneral, V. Ilyin, A. Kryukov, V. I. Savrin, A. Semenov and A. V. Sherstnev, "CompHEP 4.4: Automatic Computations From Lagrangians To Events", *Nuclear Instruments and Methods.*, Vol. A534, pp. 250–259, 2004.

26. Kersevan, B. P. and E. Richter-Was, "The Monte Carlo Event Generator AcerMC Versions 2.0 To 3.8 With Interfaces To PYTHIA 6.4, HERWIG 6.5 and ARIADNE

4.1", *Computer Physics Communications.*, Vol. 184, pp. 919–985, 2013.

27. Frixione, S., E. Laenen, P. Motylinski and B. R. Webber, "Single-Top Production In MC@NLO", *Journal Of High Energy Physics*, Vol. 0603, p. 092, 2006.

28. Becker, K., T. Cornelissen, F. Derue, A. Henrichs, D. Hirschbühl, X. Lei, O. Nackenhorst, F. O'Grady, D. Pelikan, M. Pinamonti, S. Pires, J. Sjölin and P. Tepel, *Estimation Of Fake Lepton Background For Top Analyses Using the* $\sqrt{s} = 8$ *TeV Dataset*, Tech. Rep. ATL-COM-PHYS-2013-1100, CERN, Geneva, 2013.

29. Junk, T., *Sensitivity, Exclusion, and Discovery with Small Signals, Large Backgrounds, and Large Systematic Uncertainties*, Tech. rep., FERMILAB.

30. Junk, T., "Confidence Level Computation For Combining Searches With Small Statistics", *Nuclear Instruments and Methods.*, Vol. A434, pp. 435–443, 1999.

31. Read, A. L., "Presentation Of Search Results: The CL_s Technique", *Journal of Physics G: Nuclear and Particle Physics*, Vol. 28, No. 10, p. 2693, 2002.